VOLUME 72, NUMBER 23

JOC Perspective

NOVEMBER 9, 2007

Novel Organic Materials through Control of Multichromophore Interactions

Guillermo C. Bazan

Departments of Chemistry & Biochemistry and Materials, Institute for Polymers and Organic Solids, University of California, Santa Barbara, California 93106

bazan@chem.ucsb.edu

Received June 4, 2007

The function of organic semiconducting and light-harvesting materials depends on the organization of the individual molecular components. Our group has tackled the problem of through-space delocalization via the design and synthesis of bichromphoric pairs held in close proximity by the [2.2]paracyclophane core. The linear and nonlinear optical properties of these molecules provide a challenge to theory. They are also useful in delineating the problem of intermolecular contacts in molecular conductivity measurements. Another area of research described here concerns conjugated polyelectrolytes. These macromolecules combine the properties of organic semiconductors and conventional polyelectrolytes. We have used these materials in the development of optically amplified biosensors and have also incorporated them into organic optoelectronic devices. Of particular interest to us is to derive useful structure/property relationships via molecular design that address important basic scientific problems and technological challenges.

Synthetic methods and transformations provide the route to artificial materials. Organic materials benefit from a well-stocked arsenal of specific bond-making reactions, characterization capabilities, and purification techniques developed by organic chemists and polymer scientists. A recent Perspective in this Journal provides a remarkable diversity of natural products accessed via methods and techniques that precisely determine the atomic connectivity within the three-dimensional structure of *isolated* molecules.[1] Many other examples can be found in the literature. In organic optoelectronic materials research, however, one needs to consider the condensed state, where the relative orientation and distances between the molecules determine important properties such as the mobilities of charge carriers, the emission quantum yields, and how excitations can be dissociated into charges or transferred to lower energy sites. The final organization in the bulk is determined by weak intermolecular forces, which are difficult to "program" within the internal composition of the molecules. Furthermore, one often works in nonequilibrium conditions, which are strongly influenced by the external forces applied to the system during the processing steps. The literature is replete with examples where the "morphology" of the sample is blamed for the inability to achieve an optoelectronic performance that was anticipated on the basis of molecular design.[2] Morphology here is a murky term that relates to the organization of molecular components in the bulk.[3] It may refer to crystal polymorphs, crystalline domains in polymer films, microphase separation of nonmiscible components, how molecules organize at a metallic or inorganic surfaces or interfaces, and so on. Lack of control over bulk morphology and phase separation presents the primary roadblock for increasing the performance of organic solar cells.[4]

Broad scope organic materials research is best tackled via a multidisciplinary approach. Often a hypothesis or new device concept based on a new material will be put forth for verification or testing. The synthetic chemist, for better or worse, always begins the work. "Molecules" then turn into "samples". Testing and characterization ensues. If the subsequent work is done with collaborators from a different discipline, then the discussion and communication presents a significant challenge. Much of the basis for understanding charge transport in organic semiconductors comes from contributions from solid-state physicists. Most synthetic chemists and physicists do not share the same vocabulary. Excitons are really excited states. Phonons are vibrations, while solitons are related to radical species. Perfect lattices do not exist in real conducting polymers but are the basis for understanding band transport. Organic chemists do not have the proper curriculum readily to absorb these concepts and to apply their capabilities and analytical thinking to solving

10.1021/jo071176n CCC: $37.00
Published on Web 09/21/2007

SCHEME 1. Schematic Illustration of Two Stilbene Chromophores Held in Close Proximity via the [2.2]Paracyclophane Core and the Synthesis of Pseudo-*para*-distyryl[2.2]paracyclophane ($\mathbf{1_{pp}}$)

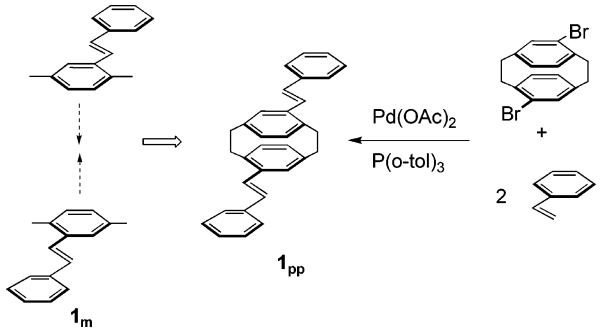

critical materials issues. Persistent effort over time is needed to overcome these language barriers, although initiatives are being made through courses specifically designed to enable students in different disciplines to communicate with each other.

This Perspective provides an account of how our group developed new organic materials targeted primarily for optoelectronic applications. The first part of the article provides an account of our work on bichromophoric systems built on the [2.2]paracyclophane structure. This effort was primarily basic science in nature. The second section provides selected examples of our work on conjugated polyelectrolytes. Here the work takes a more practical approach. However, through this effort we have been able to tackle some interesting problems concerning the self-assembly of optically active systems and the role of mobile ions in organic semiconductors. In all studies, we synthesize new molecular components that are then tested for developing a better scientific basis for correlating structure and properties or are incorporated into device structures or sensory schemes to improve performance. Throughout this contribution the emphasis is on the new molecular structures and how these are used to extract new information. Synthetic details can be found in the references.

The [2.2]Paracyclophane Story

Our initial interest started in the mid 1990s with a focus on the problem of "aggregates" in conjugated polymers used for organic light-emitting diodes.[5] These devices function by injection of electrons from a cathode (reduction) and holes from an anode (oxidation) into an organic film capable of charge transport and emission.[6] Charge recombination leads to the formation of excited states and the subsequent emission of light. Regions of the film with increased polymer order exhibit lower emission quantum yields. Because of the poorly defined nature of these aggregated regions, we set out to synthesize precisely determined molecular structures that bring together two chromophores into close proximity and would make it possible to probe the effect of orientation, contact site, and the length of electronic delocalization on the optical properties. The goal was to better understand the problems of "through-space" delocalization,[7] which are perturbations in molecular electronic structure caused by another chromophore via Dexter and/or Förster mechanism(s).[8,9] It should be noted that interchromophore electronic delocalization is not a problem unique to materials research. Consider, for example, the electronic communication between antennae and reaction centers in photosynthesis[10] and the debate on electron and hole transport along duplex DNA.[11,12]

Our strategy was to take advantage of the [2.2]paracyclophane framework[13−15] as the site of interchromophore contact[16,17] since it enforces cofacial overlap of two aromatic rings, minimizes intramolecular motion, and has proven useful for the study of $\pi-\pi$ electron delocalization and ring strain in several organic compounds. For example, [2.2]paracyclophane itself behaves as a pair of strongly interacting benzene rings and displays spectroscopic features that have been described as analogous to those of a benzene excimer.[18,19] Although drawn flat for clarity, ring strain distorts substantially the aromatic rings. The distance between bridgehead carbons on opposing rings is ~2.78 Å, while the distance between rings measured from the nonbridging carbon−carbon bonds is ~3.09 Å.[20]

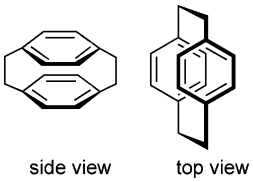

Scheme 1 illustrates the concept of chromophore dimers and provides a synthetic example. The target molecule, pseudo-*para*-distyryl[2.2]paracyclophane ($\mathbf{1_{pp}}$), may be considered as two stilbene derivatives positioned on top of each other at a distance and orientation dictated by the [2.2]paracyclophane core. Compound $\mathbf{1_{pp}}$ is obtained by treatment of pseudo-*para* dibromoparacyclophane[21] with styrene under Heck coupling conditions.[22,23] Comparison of the photophysical features of $\mathbf{1_{pp}}$ with those of the parent chromophore ($\mathbf{1_m}$) yields insight into the effect of delocalization via the transannular gap in the [2.2]paracyclophane core. One observes higher photoluminescence quantum efficiencies and more red-shifted emission for the dimeric species.

Scheme 2 provides a series of derivatives prepared to extend the concepts in Scheme 1.[24] The pseudo-*para* compound $\mathbf{2_{pp}}$ can be thought of as holding together two distyrylbenzene chromophores. Comparison of $\mathbf{1_{pp}}$ and $\mathbf{2_{pp}}$ yields information on perturbations brought about by increasing the through-bond conjugation length. In the pseudo-*ortho* isomer $\mathbf{2_{po}}$, it is possible to probe the effect of chromophore orientation. Molecule **3** is similar to $\mathbf{2_{pp}}$ and $\mathbf{2_{po}}$, except that the contact site of the distyrylbenzene chromophore is now the central ring.[25] Finally, compound **4** provides a fairly extended conjugated framework. For compounds $\mathbf{2_{pp}}$ and $\mathbf{2_{po}}$, one does not observe a substantial difference between the properties of the dimers and the constituent distyrylbenzene monomer analogues. Compounds **3** and **4** show red-shifted emission compared to the corresponding monomers.

Constructing a rationale for the structure/optical properties relationships in the class of compounds in Schemes 1 and 2 required collaboration with the research group of Professor Shaul Mukamel. The collective electronic oscillator (CEO) approach[26] demonstrated previous success at describing the optical response of chromophore aggregates. This technique computes molecular vertical excitation energies and their oscillator strengths, which allow one to infer linear absorption spectra. In addition, the transition density matrices, or electronic modes, are calculated for each excited state. These matrices show relevant electronic motion when the molecule interacts with light in real space.

The CEO method faithfully replicates the absorption and emission spectra of the molecules in Schemes 1 and 2, and a

SCHEME 2. The Molecular Structures of Compounds 2_{pp}, 2_{po}, 3, and 4

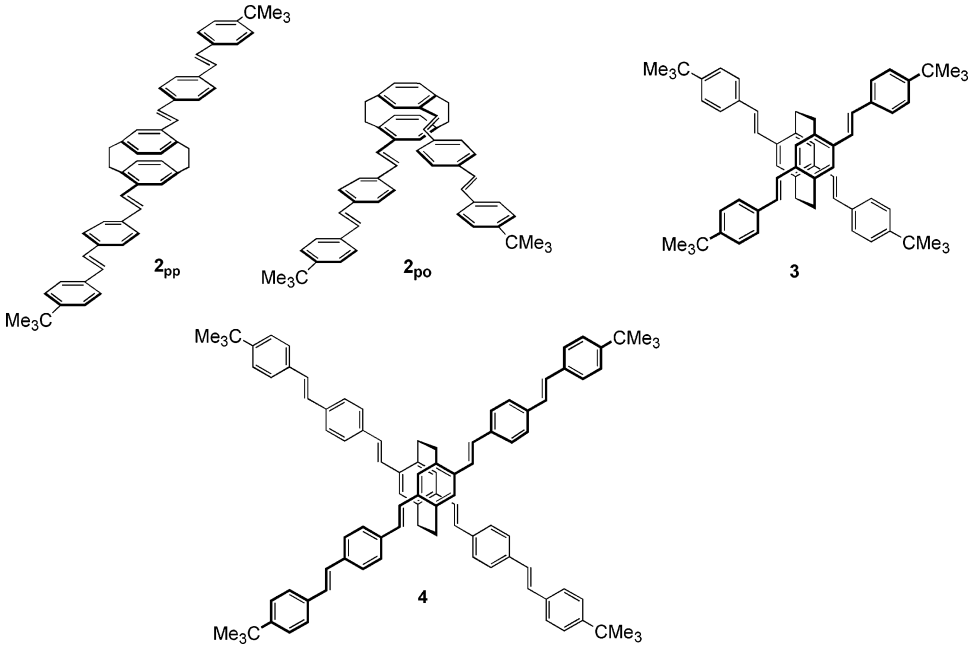

SCHEME 3. Qualitative Electronic Description of Bichromophoric [2.2]Paracyclophane Molecules

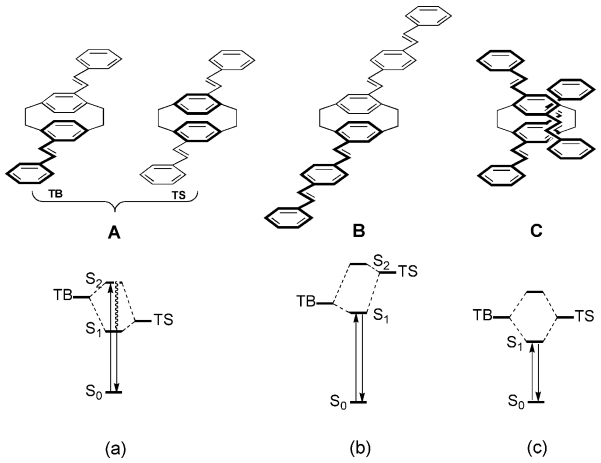

(a) In A, absorption occurs via the stilbene fragment, as shown by the excitation from S_0 to S_2. Internal conversion populates S_1, which is primarily TS in character, and emission occurs from there. (b) In B, TB is of lower energy, relative to TS. (c) The regiochemistry of the interchromophore contact in C results in an S_1 state with substantial mixing of TB and TS.

brief qualitative description of the results is provided here. One can approximate the general features using the photoexcitation dynamics in Scheme 3. Here, **TB** (through-bond) corresponds to an electronic state dominated primarily by the characteristics of the original (monomeric) chromophores. **TS** (through-space) corresponds to an electronic state that is mostly derived from the features of [2.2]paracyclophane. In the case of molecules held together via the terminal ring, the most significant absorption is attributed to the "monomer" chromophore antenna, that is, stilbene in the case of $\mathbf{1_{pp}}$ or distyrylbenzene in the case of $\mathbf{2_{pp}}$ or $\mathbf{2_{po}}$. The **TS** state has a vanishing oscillator strength. Emission from this state is broad and featureless. Two situations may be encountered after photon absorption. For $\mathbf{1_{pp}}$, the energy of the localized excitation (**TB**) is higher than that of the **TS** state (situation A in Scheme 3). Internal conversion transfers the excitation from the localized monomer, and emission takes place from **TS**. In the analogy to interchromophore contacts in the bulk, this process mimics energy migration from an individual molecule to the "aggregated" site. Emission from **TS** is described by a relatively long-lived excited state, which is consistent with the forbidden nature of this transition.

Situation B in Scheme 3 arises when the energy of **TB** is lower than the corresponding **TS**. This is the situation for distyrylbenzene (i.e., $\mathbf{2_{pp}}$ or $\mathbf{2_{po}}$). Under these circumstances, the initial excitation remains localized and there is negligible difference between the spectra of the parent chromophore and their corresponding dimers. In the case of molecules **3** and **4**, for which the contact is via the internal ring, a dissection into predominatnly **TB** and **TS** states is not possible. The CEO method indicates extensive delocalization throughout the entire molecule. This idea is illustrated in situation C in Scheme 3.

That molecules such as **3** and **4** display electronic delocalization throughout their structures makes them interesting within the context of three-dimensional conjugation. Such molecular systems are described by symmetry elements not contained within the structures of linear or two-dimensional analogues. Theoretical efforts based on group theory and quantum mechanical principles have yielded guidelines for nondipolar molecular structures, typically known as *octupolar* molecules, which are potentially useful within the context of nonlinear spectroscopies.[27] The [2.2]paracyclophane framework provides a suitable backbone in the form of a polarizable transmitting unit that is amenable for subsequent functionalization. For this effort, we collaborated with the research groups of Professors Joe Zyss and Shaul Mukamel to provide a combined synthesis, spectroscopy, and theory effort to understand the potential and limitations of higher symmetry nonlinear optical chromophores.[28]

Figure 1 shows some of our synthetic targets.[29] The disposition of donor and acceptor groups is represented in the form of a distorted cube to highlight the geometric relationships between the substituents. Substitution consisting of four donor groups provides (4,7,12,15)-tetrakis(4′-dihexylaminostyryl)[2.2]-paracyclophane (**5**) with the highest symmetry of the series. If

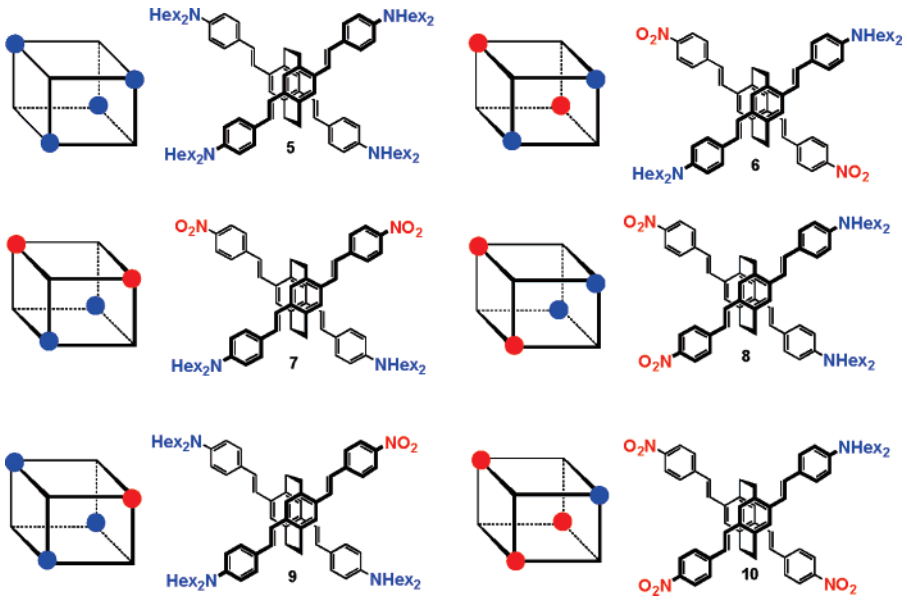

FIGURE 1. Three-dimensional tetra-donor−acceptor molecules with their respective cubic point-charge pattern.

rotational and cis/trans isomers are ignored, there are three C_2 axes leading to D_2 octupolar symmetry. This molecule can be thought of as a relatively nonfluxional dimer of symmetrical D−π−D (D = donor groups, π = delocalized bridge) chromophores with enforced cofacial overlap at the central rings.

Compounds **6**, **7**, and **8** consist of substitution with two donor groups and two acceptors but differ in their regiochemistry. All three contain one C_2 axis but are distinguished by the orientation of that unique axis with respect to internal core. Compound **6** stands out as it brings together two centrosymmetric subunits. This arrangement allows for a dipole that is oriented ring-to-ring in the [2.2]paracyclophane subunit. A striking difference between **7** and **8** on one hand and **6** on the other hand is that the former are made up of the assembly of two strongly dipolar aromatic subunits, whereas the latter consists of two nonpolar centrosymmetric subunits, albeit leading to a polar overall system. For all three, the resulting dipoles fall along the unique C_2 axis.

With replacement of a single donor group with an acceptor in **5**, all symmetry elements other than identity are lost, as in (4,7,12)-tris(4′-dihexylaminostyryl)-15-(4″-nitrostyryl)[2.2]-paracyclophane (**9**). Conceptually, this member of the series can be viewed as a D−π−A distyrylbenzene molecule brought into contact with a symmetric D−π−D chromophore. The molecule 4-(4′-dihexylaminostyryl)-(7,12,15)-tris(4″-nitrostyryl)[2.2]-paracyclophane (**10**) is analogous with **9** but with a substitutional transposition of donor and acceptor groups. This interchange leads to a molecule that, in the contact pair view, brings a D−π−A chromophore into contact with a symmetric A−π−A acceptor-type fragment.

Initial examination of nonlinear optical properties focused on 4-(4-dihexylaminostyryl)-16-(4-nitrostyryl)[2.2]paracyclophane (**11**, Figure 2).[30] This molecule was designed as a structural basis for probing how the introduction of an intermediate barrier to electron tunneling between donor and acceptor groups would influence electronic polarization properties. A combination of spectroscopic and theoretical studies showed evidence of a significant through-space charge transfer, as determined by the strong dependence of the β quadratic hyperpolarizability tensor of **11** from the additive β expected for strictly noninteracting

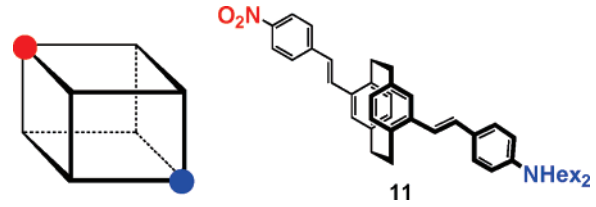

FIGURE 2. The molecular structure of 4-(4-dihexylaminostyryl)-16-(4-nitrostyryl)[2.2]paracyclophane (**11**) and the disposition of the donor and acceptor groups across the internal core.

singly substituted moieties. The desired increase of nonlinear efficiency upon substitution is not offset by the usual red shift of the absorption spectrum that limits the application of through-bond delocalized chromophores. The collective nonlinear polarization behavior involving the full structure is confirmed by the CEO approach, which indicates enhanced electron-hole delocalization in the higher order nonlinear response, compared to the linear polarizability or the static dipole moment. These findings are relevant for possible new directions for molecular design that optimizes the transparency−efficiency tradeoff in organic nonlinear chromophores.

The six permutations of donor−acceptor arrangements in Figure 1 were subsequently studied via a combination of polarized harmonic light-scattering[31] and electric field-induced second harmonic generation techniques.[32] One of our goals was to determine the contributions from the dipolar and octupolar irreducible tensor contribution to the overall β tensor value. Significant β values for molecules **5** and **6**, which are built by bringing together centrosymmetric chromophores, provide a clear signature of a purely through-space intramolecular charge transfer. However, the composite set of results showed that there is a failure of simple tensorial additivity models that focus only on the properties of the constituent units in the [2.2]paracyclophane unit. More sophisticated treatments that incorporate through-space polarization effects would be needed to fully account for the observed trends and individual properties. Additionally, the observation of a dipolar component to the quadrupolar β term indicates that vibrational and rotational

SCHEME 4. The Molecular Structures of Compounds 5m, 12m, 12, and 13

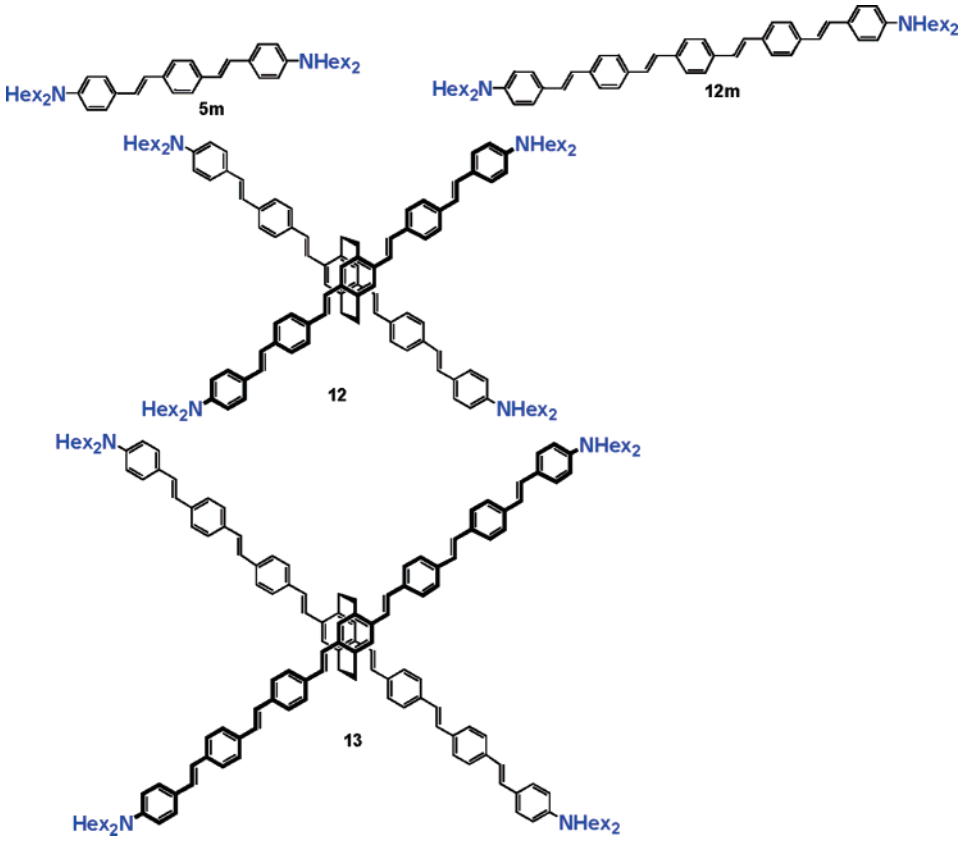

fluctuations away from the ideal geometry need to be included for an accurate correlation of optical properties with structure.

Organic molecules that exhibit large two-photon absorption (TPA) cross sections (δ) are relevant to emerging technologies such as three-dimensional optical data storage,[33,34] photodynamic therapy,[35,36] two-photon optical power limiting,[37−39] and two-photon three-dimensional microfabrication.[40−43] Coordinated synthetic, spectroscopic, and theoretical studies have yielded insight into how to better design molecules with large δ values. At the time of our studies, a successful approach had been put forth that involved a framework for mobile π-electrons with electron donor/acceptor groups on the terminal sites with or without donor/acceptor groups in the middle of the conjugated framework.[44] Such quadrupolar systems provide the potential for symmetric charge displacement upon excitation and enhanced TPA.

Having established previously the three-dimensional delocalization in the molecular systems in Figure 1, it was of interest to us to modify these molecules to address questions regarding higher symmetry effects on TPA. These studies centered on compound **5** and the chromophores **12** and **13**, as shown in Scheme 4. The monomeric species **5m** and **12m** were also included to better ascertain the effect of linking via the [2.2]-paracyclophane core on optical properties. These compounds were part of a fruitful collaboration with the research groups of Professor Joseph Perry at Georgia Tech (spectroscopy and group theory) and Dr. Sergei Tretiak at Los Alamos National Labs (quantum mechanical calculations). The combined study modeled the behavior of aggregated chromophores and examined the impact of through-space delocalization, as well as length-scaling, with the goal of providing insight and design guidelines for three-dimensional TPA chromophores.[45]

Only a summary of the optical studies and the complementary theoretical treatment is provided here. Comparison of linear absorption and TPA reveals that the through-space delocalization influences one- and two-photon excitation processes differently. One observes a characteristic Davydov splitting of the monomer band into two components in the linear absorption spectra of their respective dimers.[46] In contrast, distinct splitting is not observed in the TPA spectra of dimers, where the contributions of the monomers to the cross sections are additive. Theoretical correlation of structure with optical properties shows that this difference can be rationalized by noting that the linear and two-photon absorptions involve electronic states of different symmetries. Excited states of monomers with nearly B_u (odd) symmetry participate in the linear absorption, and near A_g (even) symmetry states participate in the TPA spectra. For the dimer states, which can be described as belonging to the D_2 point group, the strongest bands in the linear absorption spectra originate from transitions to B_2 and B_3 states. The two-photon spectrum, however, primarily contains transitions to A and B_1 states. The light induces changes of electronic density within each monomer. The electrostatic interaction between these induced charges leads to the splittings in the electronic spectra of dimers. For the dimer B_2 and B_3 states, which relate to the monomer B_u states, this interaction sums up leading to the large splittings observed in the linear absorption. In the case of dimer A and B_1 states correlating with monomer A_g states, the cancellation of individual contributions results in the vanishingly small splittings and leads to TPA spectra that are insensitive to interchromophore proximity. Studies on a wider series of compounds are necessary to assess whether the additivity in the two-photon cross section is unique to the chromophores in Scheme 4 or is more general.

SCHEME 5. Molecular Structures of Water-Soluble [2.2]Paracyclophane Dimers 14C, 15C, and 16C, Together with Their Corresponding Neutral Precursors 14N, 15N, and 16N

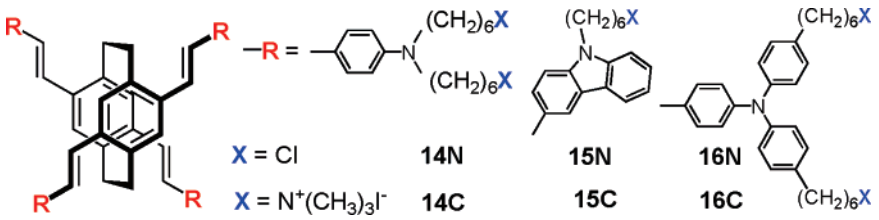

The absence of a perturbation on the characteristics of TPA chromophores upon dimerization has implications from a materials perspective when one considers that many TPA applications benefit from, or rely upon, a high density of chromophores. At high concentrations, or in the solid state, spectral positions and features of monomers in linear absorption can be superseded by absorption and emission characteristics of multichromophore systems in dimers and higher-order aggregates. Optical perturbations by aggregate formation tend to follow certain trends from the basic unit but are difficult to predict from the design of the monomer. Aggregate states are also often lower in energy and may dominate bulk behavior, regardless of their concentration. The results of this work suggest that TPA properties may be less sensitive to aggregate perturbations. It should be possible to develop a more direct link between structure−property relationships of monomers and the performance in high concentration or in solid-state applications.

Two-photon fluorescence microscopy (TPM),[47] and higher multiphoton variations, provide the best noninvasive means of fluorescence microscopy for biological imaging. The advantages of TPM have been described in detail elsewhere[48,49] and include reduced photodamage, improved depth penetration, the ability to image turbid samples, and reduced signals by the excitation beam or background cellular autofluorescence.[50] TPM-specific fluorophores for biomolecular tags are therefore an important consideration since these provide a means to further reduce photodamage and enable the use of economical laser sources. Two parameters need to be optimized for best performance. One is the two-photon absorption cross section (δ, expressed in GM $= 1 \times 10^{-50}$ cm^4·s·photon^{-1}·molecule^{-1}), which provides the probability of two-photon absorption (TPA) at a particular frequency. A large fluorescence quantum yield (η) is also desired for obtaining better signal-to-noise. The product $\eta\delta$ defines the two-photon action cross section of a molecule. Commonly used fluorescent reporters have δ values in the 1−100 GM range, which give $\eta\delta$ products of 1−50 GM.[48,51,52] As described above, it is possible to obtain much higher δ values with quasi-linear D−π−D structures. In these systems, the magnitude of δ depends on the degree of intramolecular charge transfer (ICT) upon excitation.[53] However, in polar aqueous media, the ICT leads to reduced η values and lower overall $\eta\delta$.[54,55]

Soluble [2.2]paracyclophane TPA chromophores were synthesized to examine the effect of water on $\eta\delta$. The specific molecular structures are shown in Scheme 5. The terminal groups determine the donor ability of the nitrogen atom and whether the molecule is neutral (**N** series) and soluble in nonpolar organic solvents or cationic (**C** series) and soluble in water. The overall set of compounds allows the examination of the solvent influence on δ and the effect of donor strength on η. Table 1 summarizes the absorption and photoluminescence (PL) spectra. Figure 3 shows the spectra for **16N** and **16C**, which are typical for the entire series of compounds. Neutral compounds were measured in toluene and the charged counterparts in water.

TABLE 1. Spectroscopy Summary of Compounds 14C, 15C, 16C 14N, 15N, and 16N

	solvent	λ_{abs}	λ_{em}	η^a	λ_{TPA}	δ (GM)^b
14N	toluene	434	486	0.92	725	1290
14C	water	435	553	0.04	725	370
15N	toluene	420	468	0.95	700	1690
15C	water	410	505	0.42	700	700
16N	toluene	441	492	0.92	770	2080
16C	water	431	537	0.52	750	690

[a] Measured at 10^{-6} M relative to fluorescein. [b] Peak TPA cross section at λ_{TPA}.

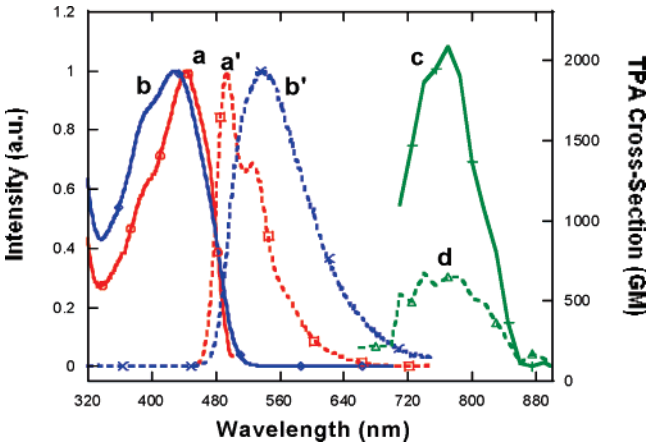

FIGURE 3. Normalized absorption and PL spectra of **16N** in toluene (a, a′) and **16C** in water (b, b′). PL spectra were collected by exciting at the λ_{abs} of each sample. TPA spectra of **16N** in toluene (c) and **16C** in water (d).

The maxima in absorption (λ_{abs}) and emission (λ_{em}) for **14N** are similar to those reported for **5**, which indicate negligible perturbation by the chloride functionalities. In toluene, **14N**, **15N**, and **16N** have high η values, in the range of 0.9. A comparison of the linear spectra of the **C** series in water with those of the **N** series in toluene reveals the following trends (Table 1). The λ_{abs} values are nearly the same (**14N**/**14C**) or slightly blue shifted (**15N**/**15C**, **16N**/**16C**). The emissions are red shifted and are broader, with no vibronic structure (Figure 3). Most importantly for the design of efficient TPM fluorophores, the η values in water are inversely proportional to the donor strength of the terminal groups (**14N** ∼ **14C** > **15N** ∼ **15C** > **16N** ∼ **16C**).[56] A drop in η is observed in for **14C** (0.04), while the η values for **15C** (0.42) and **16C** (0.52) remain high. We also note that, in a solvent of intermediate polarity (DMSO), there are no measurable differences in the linear spectroscopy

TABLE 2. Spectroscopy Summary for Compounds 14C and 16C in the Absence and Presence of SDS

	[SDS]	λ_{abs} (nm)	λ_{PL} (nm)	η^a	$\lambda_{TPA}{}^b$ (nm)	δ (GM)	$\eta\delta$ (GM)
14C	0 M	435	553	0.04	725	370	15
14C	0.05 M	434	484	0.84	730	1550	1300
14N[c]	–	434	486	0.92	725	1290	1180
16C	0 M	431	537	0.52	750	620	320
16C	0.2 mM	430	497	0.40	770	820	330
16C	0.05 M	440	488	0.95	770	2020	1920
16C	0.1 M	440	488	0.94	770	2050	1930
16N[c]	–	441	492	0.92	770	2080	1910

[a] Fluorescein (pH = 11) as a standard. [b] TPA maximum. [c] In toluene.

of the **N** and **C** series. The charged groups therefore are not interacting with the chromophores.

The TPA maximum (λ_{TPA}) and δ for **14N** in toluene (725 nm and 1290 GM, respectively) are similar to those of **5**. The λ_{TPA} values for **14N**, **15N**, and **16N** follow the trend of λ_{abs}. Compounds **15N** and **16N** have higher δ than **14N**. Literature precedent shows that arylamine donor groups in D−π−D structures can provide for larger[57] or similar cross sections, relative to alkylamine counterparts. Higher δ values may be expected on the basis of additional delocalization within the extended π electron system. Combining these results with the determination of η obtained by linear spectroscopy methods provides for $\delta\eta$ values of 294 and 359 GM for **15C** and **16C**, respectively, which are exceptionally high when compared to those of conventional TPM dyes.

Even more poorly understood than solvent effects are the perturbations by different local environments, for example, membranes, vesicles, or intracellular fluid, on $\delta\eta$. Having in our hands efficient water-soluble TPM dyes placed us in an excellent position to examine some of these problems. We focused on the effect of micelles, which are dynamic microheterogeneous structures containing surfactant molecules.[58,59] The internal structures of micelles can incorporate chromophores and thereby modify the kinetics of phosphysical processes and provide structural mimics of biological membranes.[60,61] Sodium dodecylsulfate (SDS) is a typical anionic surfactant, displays a critical micelle concentration (cmc) of 8.1 mM at 25 °C, and forms spherical micelles of low polydispersity in aqueous solution.[62]

Table 2 provides a summary of the optical changes of **14C** and **16C** observed upon SDS addition. Figure 4 compares the PL and absorption spectra in water and in the presence of SDS at concentrations above the cmc. Under these conditions, the chromophores are incorporated within the micellar cores, and the probability of finding two chromophores within a single micelle is low. There is virtually no change in λ_{abs}; however, a significant increase in the molar absorptivity of **16C** is observed. The PL spectra are blue shifted, have more pronounced vibronic definition, and larger η values are observed (0.84 for **14C** and 0.95 for **16C**), relative to measurements in the absence of SDS. These PL characteristics are similar to those obtained with **14N** and **16N** in toluene.[63]

Table 2 also contains the most significant results from TPA measurements. There is a substantial increase in δ values when one compares the results in water (δ_{max} = 370 GM for **14C**, 620 GM for **16C**) with those in the presence of 0.05 M SDS (1550 GM for **14C** and 2020 GM for **16C**). Indeed, the TPA spectra under micellar conditions are similar to the results in toluene (1290 GM for **14C**, 2080 GM for **16C**). The combined maximal $\eta\delta$ values in water when [SDS] = 0.05 M are 1300 GM for **14C** and 1920 GM for **16C**, which are more than 10 times larger than those of the current fluorescent reporters in TPM.[64] We attribute this enhancement to the incorporation of the optically active units within the hydrophobic interior of the micelles. As a result of the combined increase in δ and η, the measured $\eta\delta$ values of **14C** and **16C** are among the highest reported in an aqueous environment. Additionally, these results should be taken into consideration when examining TPM images where fluorescence intensities are used to gauge concentration of labeled substrate in biological samples. Local cell or tissue environments or microstructures may perturb substantially the optical performance of the reporter. These results also suggest that it may be possible to incorporate TPM tags within the interior of hydrophobic structures, such as dendrimers with a charged periphery[65] or polymer nanoparticles to obtain improved performance. The dependence of PL lifetime on the polarity of the medium for the [2.2]paracyclophane structures, due to participation of the forbidden states, could potentially be used as a microenvironment probe.[66]

Established methods for [2.2]paracyclophane functionalization and the theoretical framework available for understanding optical properties as a function of molecular structure and environment allowed us to begin a study that probed solvatochromism differences for through-bond and through-space delocalized states. For this study, we used **14N** and **14C**, together with the set of molecules shown in Scheme 6. Compounds **17N** and **17C** contain two distyrylbenzene chromophores without donor substituents and are neutral and charged, respectively. In the case of **18N** and **18C**, only the [2.2]paracyclophane core is optically active and they are soluble in organic solvents and water, respectively. Also included are the neutral and charged *monomer* building blocks of **14** and **17**, specifically **$14N_m$**, **$14C_m$**, **$17N_m$**, and **$17C_m$**.

With the set of compounds described in the preceding paragraph, it was possible to probe the effect of donor groups and solvent polarities on linear optical properties.[63] A brief discussion of the results follows. First of all, our hypothesis is that differences in absorption and PL spectra between structurally related monomers and dimers stem from the through-space electronic delocalization across the center ring of the distyrylbenzene structure. There are no measurable differences in the absorption or fluorescence spectra when one compares the neutral version of a molecule to its charged counterpart (i.e., **17N** vs **17C**), *in the same solvent*. The quaternary groups, together with their corresponding counterions, do not play an important role in determining the energies of the excited states. Compounds **$17N_m$** and **$17C_m$** are the most basic distyrylbenzene structures in this study, and their PL maxima (λ_{PL}) are similar when measured in toluene (**$17N_m$**) and in water (**$17C_m$**). The absence of a solvatochromic effect is consistent with a similar charge distribution of the ground state and the emitting state.[67] The values calculated for the intrinsic fluorescence lifetimes (τ_{int}) are also quite similar (1.3 ns for **$17N_m$** and 2.3 ns for **$17C_m$**). In contrast, for **17N** and **17C**, the spectra change as a function of solvent. In going from toluene to water, the λ_{PL} red shifts by approximately 42 nm (0.23 eV) and the τ_{int} increases from ~3 to ~24 ns. Therefore, by creating the possibility of delocalization between the two distyrylbenzene units across the [2.2]paracyclophane bridge, one observes an emitting state that is more sensitive to solvent polarity[68] and has a lower oscillator strength.

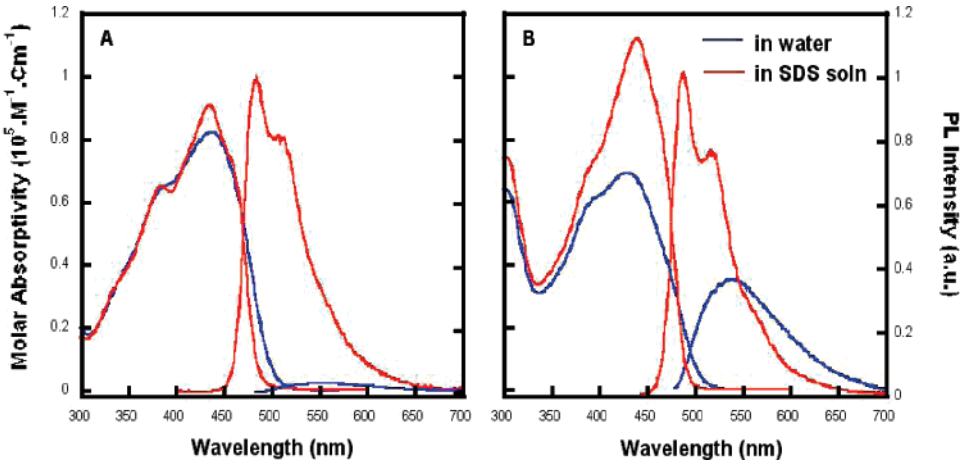

FIGURE 4. Absorption and PL spectra of **14C** (A) and **16C** (B) ([**14C** or **16C**] = 10^{-5} M and [SDS] = 0.05 M). Areas under the PL spectra are proportional to η.

SCHEME 6. Molecular Structures and Abbreviations of Compounds Used to Probe Solvatochromic Effects

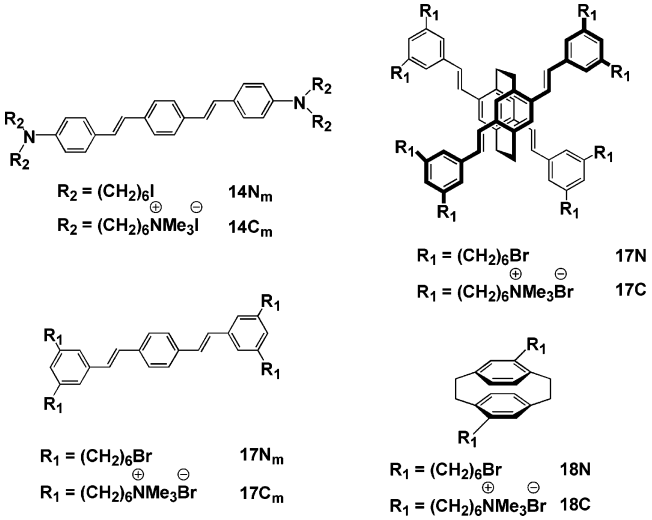

The PL spectra of **18N** and **18C**, which are essentially alkyl-substituted [2.2]paracyclophane cores, display a solvatochromic effect. Like **17N** and **17C**, neither **18N** nor **18C** have functionalities available for hydrogen bonding, which strongly suggests dependence on the solvent polarity. The λ_{PL} of **18C** in water is 7 nm (0.07 eV) red shifted relative to **18N** in hexanes, which suggests a more pronounced polarization or charge-transfer component in the emitting state relative to the ground state.

There is a strong similarity to the solvatochromism of the pyrene and naphthalene excimers, which has been studied in detail.[69] The solvent dependence of the emission frequency of these excimers,[70] in conjunction with the fact they are nonpolar,[71] indicates that the spectral shifts result from differences in polarizability between the excimer and the dissociative ground state. Extension of the results from naphthalene and pyrene excimers to the solvatochromism of **18N** implies that the excited state of **18N** is more polarizable than the ground state (which is not dissociative by virtue of its covalent structure). Similarly, for $\mathbf{17N_m}$ and $\mathbf{17C_m}$, the absence of measurable solvent dependence of the fluorescence spectra implies that the ground and emissive states have similar polarizabilities. We also note that the solvent stabilization energy as determined by the energy difference in the λ_{PL} of **18N** and **18C** in hexanes and water,

SCHEME 7. Qualitative Description of the Effect of Polar Solvents on the 17N/17C Emissive States (TB and TS Are Defined as in Scheme 3)

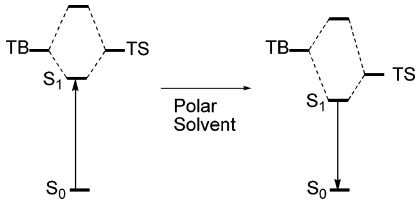

respectively (0.07 eV), is smaller than that observed in **17N**/**17C** (0.23 eV), which indicates that the polarizability in **17N**/**17C** is further enhanced through its more extended π-conjugated system.

Based on the influence of structure on solvatochromism, the previous characterization of solvent effects on aromatic excimers, the insensitivity toward solvent polarizability, and the electronic structures described in Scheme 3, it is possible to account for the dependence of the τ_{int} of **17N** and **17C** on solvent polarity, as shown in Scheme 7. In a nonpolar solvent, the description is similar to that in Scheme 3 (c), with the emitting S_1 state containing substantial **TB** and **TS** mixing. Increasing solvent polarity leaves **TB** relatively unperturbed, but lowers the **TS** energy level. As the energy difference of these states increases, the S_1 state becomes more **TS**-like and its oscillator strength decreases. Therefore, the longer τ_{int} value of **17C** in water, relative to **17N** in toluene, is due to the stabilization of **TS** and its greater participation in the description of S_1. Essentially, when solvent polarity increases, the electronic structure of the molecule becomes more like situation A in Scheme 3 (a).

For the donor containing monomers, $\mathbf{14N_m}$ and $\mathbf{14C_m}$, there is a strong solvatochromic effect. A red-shifted PL with increased solvent polarity, as well as a loss in fluorescence quantum yields, reflects the intramolecular charge-transfer character of these compounds due to the electron-rich terminal amino groups. That vibronic structure appears in the fluorescence spectra of both $\mathbf{14N_m}$ and **14N**, together with the fact that $\mathbf{14C_m}$ and **14C** have similar PL maxima and τ_{int}, indicates that S_1 is mainly described by **TB**, which is located on the donor-substituted distyrylbenzene fragment (Scheme 8).

Up to now we have discussed the utility of covalently linked chromophore pairs with respect to their relevance in unraveling

SCHEME 8. Qualitative Description of the Effect of Polar Solvents on the 14N/14C Emissive States (TB and TS Are Defined as in Scheme 3)

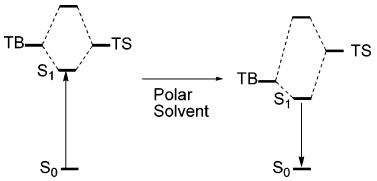

SCHEME 9. The Molecular Structures of 19 and 20

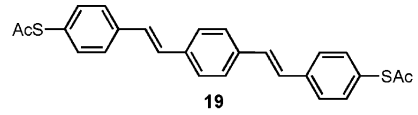

19

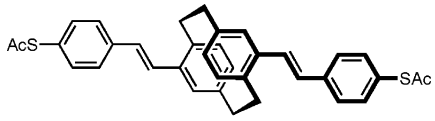

20

complex optical phenomena buried in more complex aggregated systems. The last effort reviewed here is a study on their role for understanding charge transport across a single molecule, or a single molecular layer,[72] which was done in collaboration with Dr. James Kushmerick, now at NIST.[73] These measurements give fundamental understanding and foundations for evaluating molecule-based technologies, often referred to as *molecular electronics*.[74] Experiments have demonstrated that molecules addressed in parallel act as independent conductance channels,[75−77] namely, an ensemble of molecules behaves the sum of the individual molecular conductances. Calculations predicted, however, that more facile charge transport could be achieved by a monolayer of strongly interacting conjugated molecules due to the formation of a pseudo two-dimensional band structure in the molecular layer.[78] Strong π-orbital coupling is anticipated for structures in which the intermolecular distance is reduced below 4 Å.[79] Herringbone packing structures,[80,81] typical of monolayers with rigid-rod π-conjugated molecular wires, precludes such strong $\pi-\pi$ coupling. Building an interdigitated molecular bilayer using [2.2]paracyclophane allows one to obtain the necessary strong electronic coupling while at the same time enforcing a cofacial relationship between the active units.

For this effort, we focused on the properties of 1,4-bis[4′-(acetylthio)styryl]benzene (**19**, see Scheme 9) and 4,12-bis[4′-(acetylthio)styryl[2.2]paracyclophane (**20**). Their synthesis, which has been described in detail elsewhere, relied on a strategy involving protection of the reactive thiol group as its (*S*)-methyl derivative, which is more tolerant of synthetic manipulations that require strong or nucleophilic bases.[82,83] To avoid working with the more reactive free thiols at the monolayer building stage, the (*S*)-acetyl groups can be deprotected to free thiols in situ under a nitrogen atmosphere, and the resulting solutions are then immediately exposed to gold surfaces.

A cartoon illustration of our perspective for these systems and measurements is shown in Figure 5. Monolayers of **19** and **20** are sandwiched between two gold electrodes and held in place via Au−thiol covalent bonds. In the case of **19**, conductance involves participation of the orbitals on distyrylbenzene. In the case of **20**, one can picture that each link involves two stilbene molecule that are forced to overlap through space via the [2.2]paracyclophane core. Under the appropriate experimental conditions, both **19** and **20** produce good quality monolayers with high packing densities on Au surfaces, as determined by electrochemical studies.[84] The packing density of the two monolayer films was modeled according to the van der Waals radii of the molecules.[85] These calculations showed that perfect monolayers of **19** would have approximately twice as many molecules per unit area as monolayers of **20**. These calculated packing densities were further supported by electrochemical desorption measurements which determine the molecular surface coverage from the current needed to irreversibly oxidize the molecules from the electrode.

Conductance measurements relied on the crossed-wire tunneling junction technique, which has the ability to examine charge transport[86] and inelastic electron tunneling spectroscopy[87] in a well-controlled and reproducible manner. A crossed-wire tunneling junction is formed when one 10 μm diameter gold wire, modified with a monolayer containing the molecule of interest, is brought into gentle contact with a second unmodified gold wire controlled by a small DC deflection current in the presence of an external magnetic field. Experimentally, this approach offers several advantages to other conductivity measurement techniques. Foremost, the top metal−molecule contact is made mechanically, thereby avoiding exposure of the molecules to a metal evaporation that can disturb or chemically modify the thin molecular layer. Since formation of molecular junctions in this manner is relatively easy, it is possible to repeatedly measure the sample of interest, generating multiple data sets where statistics can be applied. Although the measurements are made on an ensemble of molecules in the monolayer, previous studies have shown excellent correlation between crossed-wire measurements and single molecule STM measurements.[88]

Current−voltage ($I-V$) characteristics for molecular junctions formed from monolayers of **19** and **20** are shown in Figure 6. Both molecules yielded molecular junctions stable to repeated measurements for bias voltages in the ± 1 V range. The symmetry of the $I-V$ characteristics demonstrates that the Au−S contacts at either end of the molecules are chemically similar.[89] The most striking aspect of the $I-V$ characteristics is the high conductivity measured for **20** despite the break in π-conjugation imposed by the internal [2.2]paracyclophane core. The conductivity of Au/**19**/Au, calculated from the slope of the linear low bias region, is only 2.3 times greater than that of Au/**20**/Au. When considering that the packing density of the monolayer of **20** is approximately half the packing density of monolayer of **19**, *the conductivity per molecule for the two structures is the same given the uncertainties of the measurements.* For comparison, orders of magnitude differences in conductivity are observed between saturated alkanes and π-conjugated oligomers of similar length.[90] The similar measured $I-V$ characteristics of **19** and **20**, specifically, the magnitude of the conductance, indicate that the [2.2]paracyclophane arrangement provides an efficient mechanism for charge transport.

Delocalized orbitals that span the entire molecule and are positioned close to the Fermi level of the metal electrodes facilitate charge transport across molecular junctions.[91] To evaluate the potential conductance channels, the electronic structure of molecules **19** and **20** were calculated at the B3LYP/LANL2DZ level of DFT theory with single Au atoms attached to the terminal S atoms on either side of the molecule. The

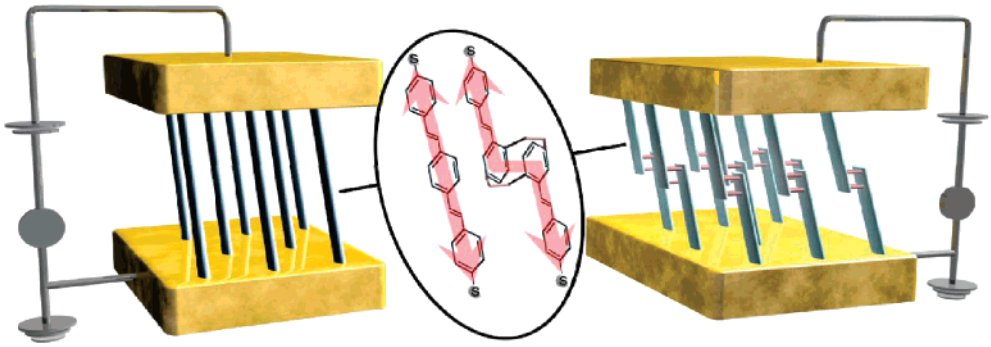

FIGURE 5. Schematic illustration of the situations encountered when probing monolayers of **19** and **20**.

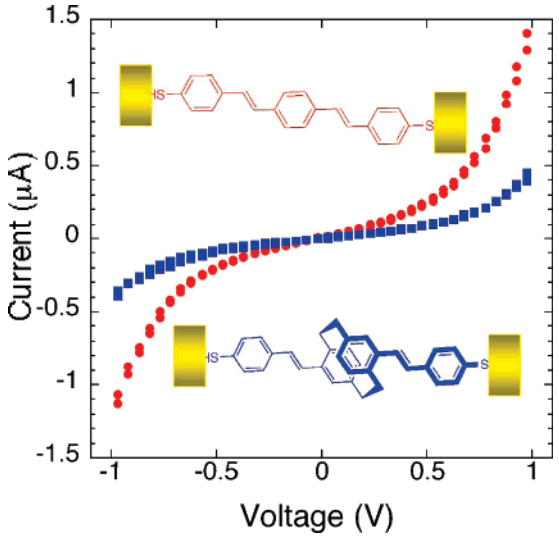

FIGURE 6. Linear scale $I-V$ characteristics for Au/**19**/Au (red) and Au/**20**/Au (blue) averaged from three independently formed junctions.

calculated charge density plots of **20** demonstrate that, although there is a break in through-bond conjugation at the [2.2]-paracyclophane core, the π-system of the two coordinated stilbene units spans the entire molecule due to through-space conjugation. The HOMO-1 in **20** demonstrates delocalization across the π-system and is similar in energy to the HOMO energy of **19** (-5.8 and -5.6 eV, respectively); both are close to the Fermi level of Au (-5.31 eV).[92] The similar conductivity is thus likely due to charge transport through energetically similar filled molecular orbitals. From a larger perspective, the high conductance of **20** indicates that suitably arranged π-systems can exhibit strong through-space $\pi-\pi$ coupling for charge transport. While it is currently difficult to imagine how one could drive a monolayer system to adopt such molecular packing, this result should provide motivation for such research as well as for designing future molecular species that incorporate multiple appropriately coordinated conjugated subunits.

We conclude this section of the Perspective by looking at insight obtained using **19** and **20** for comparing and correlating molecular transconductance measurements by different experimental techniques. The possibility of using individual organic molecules for molecular-scale electronic applications has prompted the development of numerous techniques to measure the charge-transport properties of a few or single molecules[93−97] or self-assembled monolayers (SAMs).[90,98,99] In addition to these ensemble measurements, a number of methods have been developed that contact and measure the charge transport of individual molecules.[100−102] It is of obvious importance to ensure that these methods provide structure/property relationships that can be related to each other and to understand the role that the intrinsic electronic properties of the organic can play in these correlations. Our efforts focused on a comparison of the tunneling decay constant, determined from scanning tunneling microscopy (STM) imaging, with metal−molecule−metal conductivity measurements, obtained from conductive atomic force microscopy (C-AFM) measurements, for single molecules isolated in an alkane thiol matrix.

Because of space limitations, the discussion will be brief and only highlights will be presented, primarily at a qualitative level. The test samples involved two-component SAMs formed by inserting **19** or **20** into a monolayer of undecanethiol on Au(111). Under these conditions, the conjugated molecules are inserted into the matrix film at step edges and domain boundaries where it has been demonstrated that they are electronically isolated and exist in an upright fashion due to the rigidity of the supporting monolayer matrix.[103] For STM measurements, images were collected with the tip biased under constant current feedback control. The delocalized electronic structures of **19** or **20** result in bright spots in the image due to differences in both their physical height and their electronic properties relative to the alkane monolayer. Deconvolution of variables and comparison against the background matrix using the formalism by Weiss and co-workers[104] yields β, the tunneling decay constant, which is related to the electronic properties of the molecule. This analysis provided β values of 0.40 ± 0.12 and 1.16 ± 0.25 Å^{-1} for **19** and **20**, respectively. These data would indicate a higher molecular conductivity for **19**, relative to **20**, *in contrast to the results obtained using cross-wire junction measurements shown in Figure 6.*

Molecular conductivity measurements were done using C-AFM. Monolayers containing inserted **19** or **20** were functionalized with gold colloids through attachment to their unbound protruding thiol functionality by soaking the two-component SAMs in a solution of gold nanoparticles with an average diameter of 5 nm. The inserted molecules were visualized from AFM imaging by the appearance of their attached colloids. A closed-loop $x-y$ piezo scanner was used to position the conductive tip directly over the gold colloids, and the current−voltage ($I-V$) characteristics were directly measured in the ± 1 V potential range. The relative conductivities of the molecules, calculated from the slope of the linear low bias regime and normalized to another molecular system, were 29 ± 13 and 25

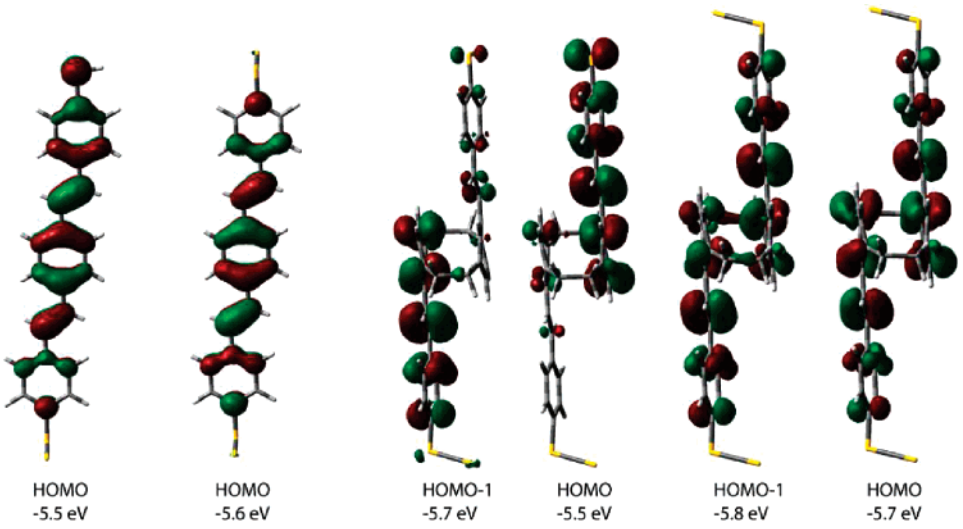

FIGURE 7. Charge density plots of the highest occupied molecular orbitals for **1** and **2** attached to one and two gold atoms (Au/**19**, Au/**19**/Au, Au/**20**, and Au/**20**/Au, respectively).

± 10 for **19** and **20**, respectively. *This result is in agreement with cross-wire junction measurements and differs from the analysis of STM images.*

Discrepancies between the measurement techniques proved to be related to the difference in the contacts that the molecules experience in the two measurements. In the AFM experiment, both thiol functionalities are chemically bound to a gold surface, while in the STM measurements, only one of the thiol end groups is attached. Electronic structure calculations were performed on **19** and **20** bound to one and two Au contacts within the density functional theory approximation (Figure 7). Single Au atoms attached to the thiol groups were used to represent the molecule/electrode interaction. Calculations reveal similar topologies for the HOMO, whether **19** is bound to gold via one (Au/**19**) or both (Au/**1**/Au) thiol groups. In contrast, the HOMO and HOMO-1 of **20** with two Au atoms (Au/**20**/Au) has a fully delocalized electronic structure that extends across the length of the molecule, but the HOMO and HOMO-1 of the singly bound Au/**20** molecule lacks these features. Specifically, the spatial degeneracy of the HOMO and HOMO-1 orbitals is lifted by the single Au contact and the charge density is localized on the upper and lower π-conjugated fragment, respectively. Such localization of the formerly continuous conduction channel highlights why the singly bound molecule (STM conditions) has such drastically different charge transport characteristics when compared to the doubly bound (C-AFM conditions) species. In the STM measurements, the tunneling charge carrier has a further distance to travel (experiences a wider tunnel barrier) before reaching the delocalized molecular orbital. It is interesting to speculate that the decreased conductance of **20** that results from a single contact is related to the observation that the through-space delocalization is more polarizable, as surmised from solvatochromic trends.

To summarize, the work on [2.2]paracyclophane structures that mimic contacts between π-conjugated molecules provides a versatile tool to probe a variety of optical and electronic properties that are embedded within the complex mixture of sites characteristic of organic materials. Admittedly, because of synthetic limitations, it is not possible to address structures that may be envisioned, particularly in amorphous systems. These dimers are nonetheless microcosms that are perfectly defined, and through their characterization, they challenge our current theoretical understanding of electronic coupling in multichromophore assemblies.

Problems and Opportunities with Conjugated Polyelectrolytes

Conjugated polyelectrolytes are polymers containing a π-conjugated backbone and functional groups that ionize in high dielectric media (i.e., salts).[105] These materials combine the semiconducting and photon harvesting properties of electronically delocalized polymers with the charge-mediated behavior of polyelectrolytes. Studying conjugated polyelectrolytes presents a common and quite different problem compared to [2.2]-paracyclophane-based bichromophoric pairs: one loses much of the certainty on the distance and orientations of the optically active units. Aggregates form in water as a result of the hydrophobic polymer backbone.[106] The internal structures within the aggregates coordinate the collective behavior of multiple chromophores and determine observables.[107] Much of the interest in conjugated polyelectrolytes is in the development of biosensors where the ultimate objective is to generate assays that detect target species in as low a concentration as possible. This drive causes one to work under conditions where common characterization techniques, such as dynamic light scattering, are not sufficiently sensitive. Incorporation into an optoelectronic device and evaluation of the resulting performance provide a composite picture of many interrelated variables where the properties of the organic component may not be dominant. Unlike neutral conjugated polymers, the ions are mobile and can redistribute applied electric fields, bringing in the problem of reconciling electrochemical and solid-state physics concepts. One therefore needs to work under conditions where the impact of molecular design is less certain. Despite these complications, conjugated polyelectrolytes have made substantial impact in diverse applications and molecular engineering is a primary component of the research.

Biosensor Applications. Our group placed substantial efforts on the development of homogeneous and heterogeneous biosensor assays that take advantage of the optical amplification afforded by conjugated polyelectrolytes.[108] The ionic groups are

SCHEME 10. The Molecular Structure of 21

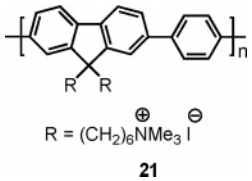

SCHEME 11. Schematic Illustration of the DNA Assay Using 21 (shown in Green) and PNA-C* (Shown in Blue, Where C* Is Fl): The System Responds Depending on Whether the ssDNA (Shown in Red) is Complementary or Noncomplementary to the PNA Sequence (Reproduced from Ref 114)

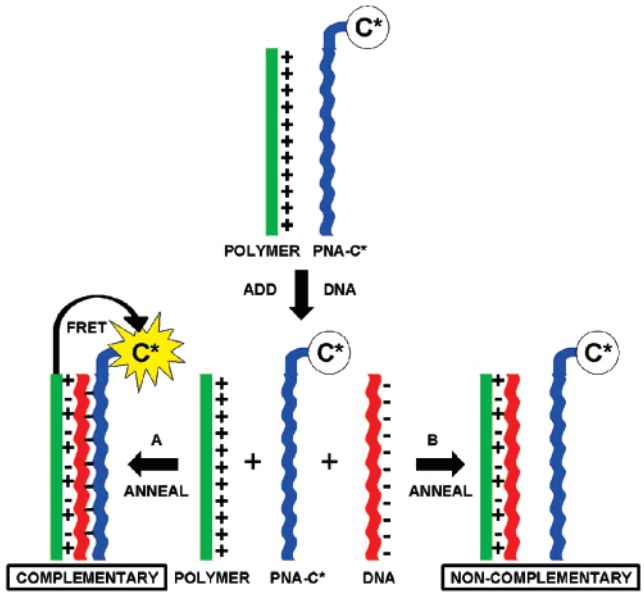

essential for increasing water solubility, an important requirement for biological detection.[109,110] The primary structures we focus on are charged poly(fluorene) derivatives and, more commonly, poly(fluorene) copolymers. Such polymers show some of the highest emission quantum yields in aqueous media, are readily prepared via Suzuki cross-coupling polymerizations, and their structures can be readily varied via substitutions at the fluorene C9 position.

Biosensors are devices that transduce a biological recognition event (such as antibody−antigen binding) into measurable signals.[111] A particular function of conjugated polymers is to amplify the signals so that lower concentrations of analyte can be interrogated.[112] Within the context of water-soluble poly(fluorenes), their action has been primarily to amplify fluorescent signatures. This amplification is the result of a higher optical cross section of the polymer, relative to small molecule reporters, and efficient fluorescence resonance energy transfer (FRET) to a signaling chromophore that is triggered upon specific molecular recognition events. Recognition specificity is paramount in view of the highly responsive fluorescence from conjugated polyelectrolytes. Examination of a limited set of variables can lead to misinterpretation of results.[113]

Our initial success was based on the optical amplification of fluorescent DNA assays using the poly(fluorene-*co*-phenylene) derivative **21** (Scheme 10).[114] As shown by the simplified illustration in Scheme 11, the detection method comprises two components: (a) the light-harvesting luminescent conjugated polymer **21** and (b) a probe oligonucleotide consisting of a peptide nucleic acid (PNA) labeled with a reporter dye such as fluorescein (PNA-Fl). Addition to the solution of a target polynucleotide with a sequence complementary to the PNA strand yields the duplex structure. Electrostatic interactions bring the conjugated polyelectrolyte into close proximity to the PNA/ssDNA-Fl duplex, resulting in FRET from the polymer to the signaling chromophore. When a nontarget polynucleotide is added, complexation between **21** and the probe oligonucleotide does not occur. Under these circumstances, the Fl remains bound to a neutral macromolecule, there is no electrostatic binding to **21**, and the average distance between **21** and the signaling chromophore is too large for effective FRET. It is possible to differentiate complementary and noncomplementary ssDNA by excitation of the polymer and measuring the Fl emission. More importantly, because the optical density of the polymer is much larger than that of Fl, and FRET is efficient, one can see up to 100-fold increase of Fl emission, compared with that obtained upon direct excitation at the absorption maximum of Fl.

By adding an S1 nuclease enzyme, it is possible to modify Scheme 11 so that the overall assay is sensitive to single nucleotide polymorphisms. The overall strategy is illustrated in Scheme 12.[115] The recognition is accomplished by sequence-specific hybridization between the uncharged, PNA-Fl probe and the ssDNA sequence of interest. Treatment with S1 nuclease leads to digestion of DNA, except for those regions "protected" by a perfectly matching hybridized PNA. The polymer **21** can function as an excitation donor to Fl only when in the PNA/ssDNA duplex. The overall method was tested by measuring the ability of the sensor system to detect normal, wild type, human DNA sequences, as opposed to sequences containing a single base mutation. Specifically, the PNA probe was complementary to a region of the gene encoding the microtubule associated protein tau.[116] The probe sequence covers a known point mutation implicated in a dominant neurodegenerative dementia known as FTDP-17, which has clinical and molecular similarities to Alzheimer's disease. Using an appropriate PNA probe, unambiguous FRET signaling is achieved for only the wild type DNA and not the mutant sequence harboring the single nucleotide polymorphism.

The general basis for the function in Scheme 11 is that upon recognition the signaling dye becomes attached to a macromolecule of net negative charge. By virtue of electrostatic attraction, the distance requirement for FRET is met and excitation of the conjugated polyelectrolyte leads to emission from the dye on the probe molecule. This approach is general and has been applied using RNA/peptide,[117] DNA/DNA,[118,119] PNA/dsDNA,[120] and RNA/RNA[121] recognition pairs. Furthermore, it is possible to adapt the process to solid-state sensors, where PNA decorated surfaces become negatively charged upon ssDNA hybridazation.[122] In the next couple of examples, we highlight that, despite the success in designing sensory schemes, much complexity exists, particularly on the coupling of the optical components and how the local structure within the conjugated polyelectrolyte aggregates influences the net output from sensory schemes.

As shown by Förster,[123] dipole−dipole interactions lead to long-range resonance energy transfer from a donor chromophore to an acceptor chromophore. Equation 1 describes how the FRET rate changes as a function of the donor−acceptor distance (r), the orientation factor (κ), and the overlap integral ($J(\lambda)$), which expresses the spectral overlap of the donor emission and

SCHEME 12. Long ssDNA Target Sequences (black) are Digested by S1 Nuclease, Leaving Intact Only Those Regions Bound to the PNA Probe (red)[a]

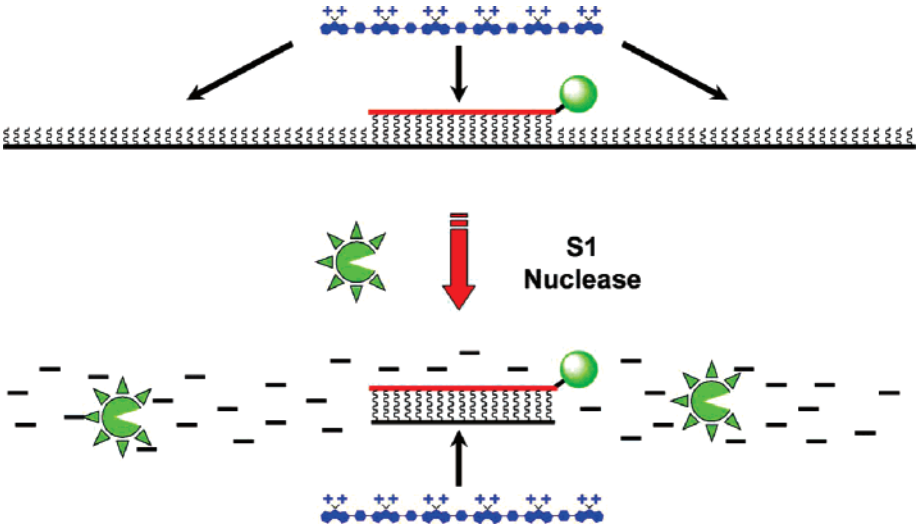

[a] **21** (blue) added directly to the resulting solutions can only associate with the remaining PNA-Fl/DNA duplex. Any PNA/DNA mismatches will result in complete DNA digestion; therefore, energy transfer from **21** occurs only for the perfect PNA-Fl/DNA complement (reproduced from ref 115).

the acceptor absorption. The FRET efficiency falls off with the sixth power of distance, and thus the modulation of energy-transfer processes provides a ready means for signal generation.

$$k_{t(r)} \propto \frac{1}{r^6}\kappa^2 J(\lambda) \qquad (1)$$

In FRET-based assays, the light-harvesting conjugated polymer and a fluorophore capable of introduction into a probe structure are generally designed to function as the donor and the acceptor, respectively. The overlap integral expresses the spectral overlap between the emission of the donor and the absorption of the acceptor. The components of the sensor can be chosen so that their optical properties meet this requirement.

A competing mechanism to FRET is photoinduced charge transfer (PCT). While PCT provides the basis for assays that modulate emission intensity, it constitutes an energy-wasting scheme in FRET assays that reduces the intensity of signals and the overall sensitivity. The rate for PCT shows an exponential dependence on the donor acceptor distance (r), that is, $k_{PCT} \propto \exp(-\beta/r)$, where β reflects the electronic coupling. Thus, there is a more acute distance dependence relative to eq 1, and as we will discuss in a subsequent section, the chemical structure of the polymer can make a strong impact on the contribution of the two processes with a given fluorophore reporter.

Scheme 13 provides a simplified illustration of two situations that may occur upon excitation of the polymer donor.[124] Situation A corresponds to the ideal situation for FRET, where the HOMO and LUMO energy levels of the acceptor are located within the orbital energy levels of the donor. Upon excitation of the donor, energy transfer to the acceptor takes place, leading to an emissive process, provided that the emission quantum yield of the acceptor is sufficiently large. Similarly, direct excitation of the acceptor under situation A does not quench the acceptor emission. When the energy levels of the acceptor are not contained within the orbital energies of the donor, in other words, when both the electron affinity and the ionization potential are higher in one of the optical partners, as in situation

SCHEME 13. Effect of Relative Orbital Energy Levels on FRET versus PCT Preferences

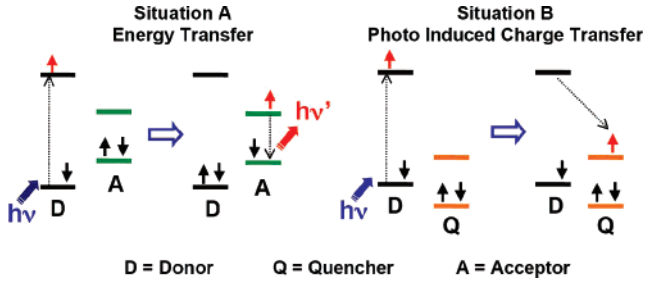

B, donor excitation may lead to PCT.[125] As shown in Scheme 13, donor excitation would lead to photoinduced electron transfer to the acceptor. Excitation of the acceptor would lead to a similar charge-separated state via hole transfer to the donor. While Scheme 13 is widely used for choosing suitable optical partners for a specific application, it fails to be accurate for intermediate cases since it neglects contributions from the exciton binding energy, the intermolecular charge transfer state energy, and the stabilization of the charged species by the medium. The mechanism by which FRET or PCT is preferred is complex for conjugated polymer blends and may involve geminate electron-hole pairs that may convert to exciplexes and ultimately excitons.[126] Despite these uncertainties, Scheme 13B provides for a necessary, but not sufficient, condition for PCT.

A series of cationic poly(fluorene-*co*-phenylene) derivatives was designed and synthesized to probe the effect of the molecular orbital energy levels on FRET efficiency.[127] As shown in Scheme 14, the molecular structures contained the parent phenylene unit (**22**) and variations bearing electron-donating (OMe, **23**) or -withdrawing (F, **24**) substituents. Compounds **21** and **22** differ with respect to the halide counterions, I^- and Br^-, respectively. As shown in Figure 8, the PL spectra of the three polymers are similar; furthermore, they all exhibit nearly identical PL quantum yields. Figure 8 also shows the absorbance of two typical dyes used in labeling probe single-stranded DNAs (ssDNAs), namely, fluorescein (Fl) and Texas Red (TR). There is much better spectral overlap between the absorption of Fl

SCHEME 14. Molecular Structures of 22, 23, and 24

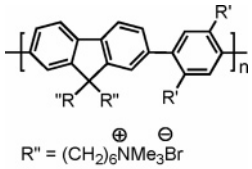

22 R' = H
23 R' = OMe
24 R' = F

and the emission of polymers **22**, **23**, and **24**, relative to the situation with TR. By looking at eq 1, one would estimate nearly identical donor capabilities for the three polymers and that Fl would be a better acceptor, relative to TR.

FRET experiments were performed by monitoring dye emission upon excitation of **22**, **23**, and **24** under conditions relevant for biosensor applications, and the results are summarized in Figure 9. Most intense Fl emission was observed for **24**/ssDNA-Fl and is approximately 2-fold more intense than that observed for **22**/ssDNA-Fl and is over an order of magnitude larger than that for **23**/ssDNA-Fl. For **24**/ssDNA-Fl, the integrated Fl emission is approximately 5-fold greater than that obtained by direct excitation of Fl at its absorption maximum (495 nm) in the *absence* of the polymers, while over 20-fold enhancement is observed relative to direct Fl excitation in the *presence* of **24**. This enhancement reflects the signal amplification provided by the light-harvesting capabilities of the poly(fluorene-*co*-phenylene) backbone. FRET experiments using ssDNA-TR show that TR emission intensities are similar for **22**/ssDNA-TR and **24**/ssDNA-TR, which are approximately twice more intense than that observed with **23**/ssDNA-TR. Of particular significance is that *the TR emission with **23**/ssDNA-TR is more intense than the Fl emission with **23**/ssDNA-Fl, despite the less effective spectral overlap* ($J(\lambda)$ in eq 1). The standard FRET equation therefore fails to provide a useful guideline to understand the complete picture of optical coupling in these systems.

Additional experiments with **22**, **23**, **24** ssDNA-Fl, and ssDNA-TR revealed the following observations. First, there is self-quenching of the dyes within the conjugated polyelectrolyte/ssDNA-Fl (or ssDNA-TR) aggregates. This effect can be diminished by including unlabeled ssDNA and is less severe for TR than for Fl. Second, there is self-quenching of the

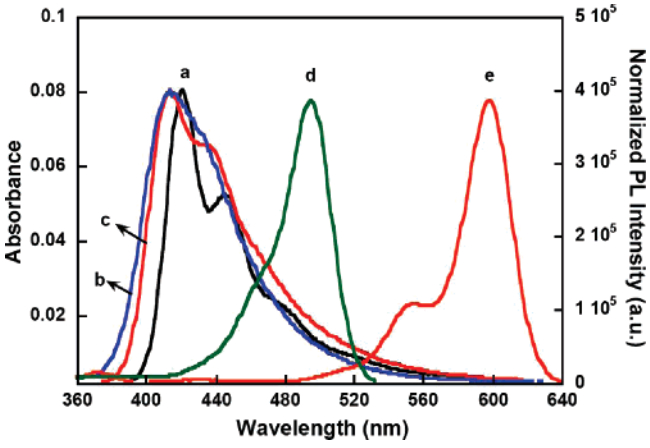

FIGURE 8. Photoluminescence (PL) spectra of **22** (a), **23** (b), and **24** (c) and absorbance of ssDNA-C* (Fl, d and TR, e) in 25 mM phosphate buffer (pH = 7.4).

polymer emission upon aggregation with unlabeled ssDNA. Third, the three polymers are quenched to the same extent with ssDNA-Fl. In other words, the chemical nature of the dyes at the terminus of the ssDNA does not appear to influence the general arrangement of the components so vastly that different optical coupling occurs. Thus, the differences in the sensitization of Fl or TR cannot be attributed to different abilities of the polymers to serve as FRET donors.

Examination of the absolute energy levels of the three polymers sheds light into the differences of dye sensitization. Cyclic voltammetry was coupled with optical measurements to estimate the HOMO and LUMO energy levels. Fluorine substitution lowers the energy levels, while the electron-donating methoxy group raises the levels, relative to the unsubstituted parent structure **22**. The Fl LUMO energy is contained within the HOMO−LUMO gap of the three polymers. However, the Fl HOMO energy (−5.9 eV) is lower than those of **22** (−5.6 eV) and **23** (−5.4 eV). For these two structures, it is reasonable to expect that situation B in Scheme 13, that is, PCT to the LUMO of Fl, is taking place. For polymer **24**, with a HOMO energy of −5.8 eV, the situation is less certain and, given the limitations of Scheme 13, both processes may be taking place to some extent. The TR HOMO level (−5.4 eV) is higher than those of **22** and **24** and is close in energy to the level of **23**. In fact, the HOMO−LUMO levels of TR are well contained between the levels of **24**, as in situation A in Scheme 13 which favors FRET over PCT. Additionally, that the energy gap difference between TR and the three conjugated polyelectrolytes is smaller than that observed with Fl likely provides additional driving force for energy transfer, relative to charge transfer.

Similar comparisons of FRET efficiencies were carried out with poly(9,9′-bis(6-*N*,*N*,*N*-trimethylammoniumhexyl)fluorene-*alt*-1,4-(2,5-bis(6-*N*,*N*,*N*-trimethylammoniumhexyloxy))-phenylene) tetrabromide (**25**) and poly((10,10′-bis(6-*N*,*N*,*N*-trimethylammoniumhexyl)-10H-spiro(anthracene-9,9′-fluorene))-*alt*-1,4-(2,5-bis(6-*N*,*N*,*N*-trimethylammoniumhexyloxy))phenylene) tetrabromide (**26**); structures can be found in Scheme 15.[128] The 10*H*-spiroanthracenyl group is orthogonal to the main conjugated backbone vector and was not anticipated to contribute to electron delocalization. These groups behave as "molecular bumpers" that effectively shield the backbone. Accordingly, both **25** and **26** show similar absorption and PL spectra, and their HOMO and LUMO levels were nearly identical, as determined by electrochemical measurements. The PL quantum yields are also identical within experimental error.

Polymers **25** and **26** were examined as excitation donors to ssDNA-Fl. Similar levels of polymer emission quenching are observed upon addition of ssDNA-Fl; however, the fate of the excitations is very different. In the case of **25**, one observes negligible Fl emission, whereas for **26**, it is possible to observe Fl emission with a FRET efficiency of 60%. Since the optical properties and orbital energy levels of for **25** and **26** are identical, the arguments presented for polymers **22**, **23**, and **24** are not applicable to rationalize the differences in optical output. However, it is important to recall that FRET and PCT rates, and thereby their probabilities, depend to different extents on the donor−acceptor distance. PCT is essentially a contact process described by an exponential distance dependence[129] and functions effectively at D−A distances considerably shorter than those probed by FRET processes.[130] The nearly complete Fl emission quenching in **25**/ssDNA-Fl suggests that polymer excitation results in PCT to Fl.[131] With **26**/DNA-Fl, one observes

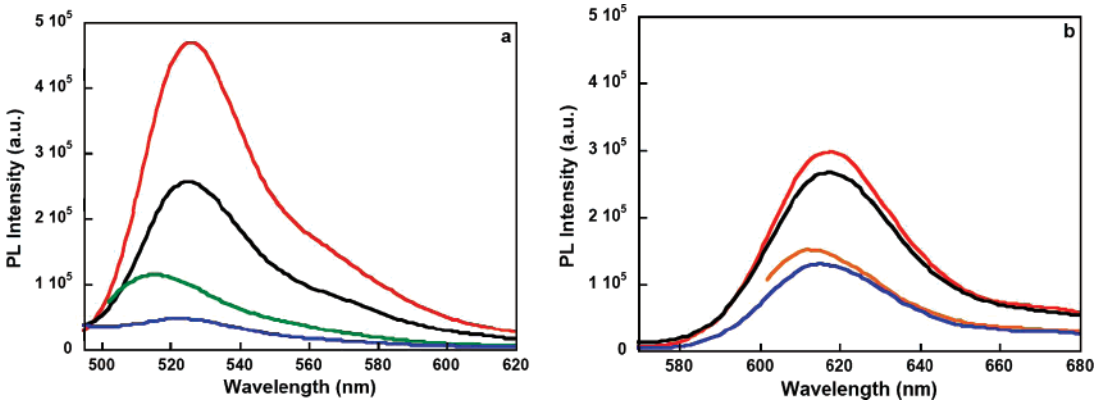

FIGURE 9. Fluorescence spectra of ssDNA-Fl (a) and ssDNA-TR (b) in the presence of **22** (black), **23** (blue), and **24** (red) in 25 mmol phosphate buffer at [ssDNA-Fl or ssDNA-TR] = 2×10^{-8} M and [RU] = 4×10^{-7} M (RU corresponds the polymer repeat unit). For each, the excitation wavelengths are at the polymer absorption maximum. Direct excitation of ssDNA-Fl and ssDNA-TR *prior* to polymer addition are also shown in green and orange, respectively.

SCHEME 15. Molecular Structures of 25 and 26

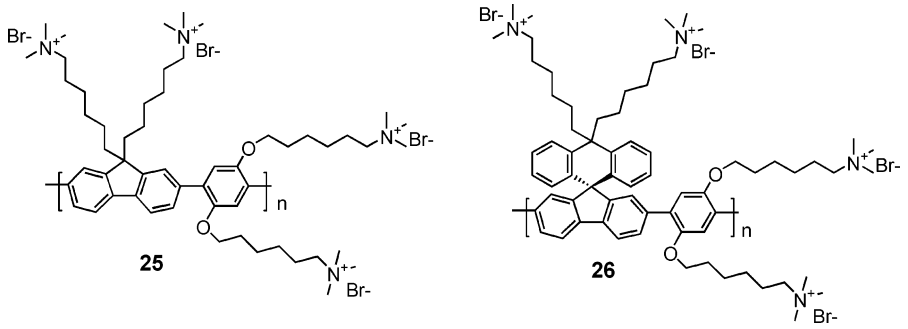

much less Fl quenching. The introduction of the molecular bumpers in **26** increases the average donor acceptor distance. This increased separation reduces the probability of PCT, relative to the parent **25** structure, but allows FRET to occur with good efficiency. These results indicate that careful attention needs to be paid to molecular design strategies that fine-tune distances at subnanoscale levels to favor FRET over quenching by PCT mechanisms.

Applications in Optoelectronic Devices. Conjugated polymers offer the opportunity of fabricating polymer light-emitting diodes (PLEDs) using solution methods. However, multilayer fabrication is challenging if all the components display similar solubilities. Depositing a new polymer can lead to removal of the underlying layer and/or mixing of the components. Conjugated polyelectrolytes are helpful in this context since their charged groups increase their solubility in polar solvents, such as water or methanol, compared to neutral structures.[132] The charged groups offer additional possibilities not accessible to their neutral counterparts. For example, dipoles may form at the metal/organic interface that raise the effective work function of the metal.[133] Additionally, the charge-compensating ions can migrate under an applied electric field, thereby balancing injected charge carriers or allowing for a redistribution of the internal electric field.[134]

In PLEDs, electrons are injected from the cathode into the π^*-band (LUMO) of the organic semiconductor, and holes are injected from the anode into the π-band (HOMO). If the work function of the cathode is greater than the π^*-band or the work function of the anode is less than the π-band, these differences lead to charge injection barriers. Because of these barriers, the current is limited to a first approximation by a combination of Fowler−Nordheim tunneling and thermionic emission mechanisms.[135] These barriers reduce device power efficiencies by increasing the turn on voltage and creating unbalanced charge injection. This problem provides a substantial obstacle to using organic LEDs in solid-state lighting applications.

A challenge thus lies in reducing the electron injection barrier. Using low work function metals, such as Ca or Ba, can effectively reduce the barrier, but these metals tend to be environmentally unstable which lowers device lifetime and requires encapsulation that minimizes penetration and deterioration by oxygen or water. Devices with multiple layer architectures can display improved efficiencies.[136] Electron transport/injection layers (ETLs) reduce injection barriers by a variety of mechanisms, including placing a dipole adjacent to the cathode,[137] band bending using doped ETLs to create ohmic (low barrier) contacts,[138] or through a series of energetically cascading layers.[139] ETLs with high electron mobilities can move the charge recombination region away from the cathode, where excitons (excited states) can be quenched.[140] ETLs can also be used as blocking layers that prevent holes from migrating across the device without recombining, forces the recombination profile away from the cathode, and alters the internal field distribution.[141]

Our initial efforts, in collaboration with the group of Professor Alan Heeger, involving incorporation of conjugated polyelectrolytes into PLED structures centered on the design and synthesis of poly{[9,9-bis(6′-(*N*,*N*,*N*-trimethylammonium)hexyliodide)fluorene-2,7-diyl]-*alt*-[2,5-bis(*p*-phenylene)-1,3,4-oxadiazole]} (**27** in Scheme 16). The idea was to incorporate the

SCHEME 16. The Molecular Structure of 27

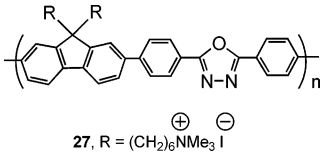

oxadiazole heterocycle into the backbone since several derivatives had been widely used as ETLs or hole blocking layers (HBLs).[132] Polymer **27** was coated from a methanol solution on top of neutral conjugated polymer layers with no interfacial mixing or deterioration of underlying layers. Significant improvements in blue-, green-, and red-emitting devices were demonstrated.

By extending the strategy of casting from solvents of different polarities to oligomers and multicomponent nonionic blends of conjugated polymers, we demonstrated the fabrication of multilayer PLEDs with white emission, high efficiency, and good color stability.[142] Such devices have the potential to be more efficient than conventional light sources and may provide substantial energy savings. A general description of the device and the molecular components of each layer is shown in Figure 10. The choice of materials includes a sulfonated oxadiazole for the ETL, a blend containing poly(fluorene), poly(fluorene) with fluorenone defects, and an iridium phosphorescent species for blue, green, and red emission, respectively, and an anionic version of poly(vinylcarbazole) for the hole injection layer (HIL). A key element of the emitting layer is the fact that the three components contain alkylated fluorene groups to minimize the tendency for phase separation. The cathode was barium, and the anode was indium tin oxide (ITO) coated with poly(3,4-ethylenedioxythiophene)poly(styrenesulfonate) (PEDOT).

The performance and general idea behind the white-emitting PLEDs shown in Figure 10 are well-established and reliable. However, our initial expectation that it was important to include organic units previously used as ETLs into the conjugated polyelectrolyte design proved to be unnecessary. Literature reports showed that simpler structures function well in this respect. It was proposed that the insertion of charged or polar groups adjacent to the cathode results in a positive interfacial dipole that effectively lowers the work function of metals such

SCHEME 17. The Molecular Structure of 28 and the Corresponding Anions

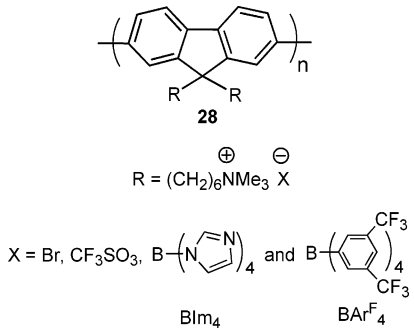

as Al or Au[133] and results in a lowering of injection barrier heights at the interface. However, the orientation and dynamics of charged groups at the metal/polymer interface remained poorly understood. We thus set out to examine how the charge-compensating anions of the cationic poly([(9,9-bis(6′-*N*,*N*,*N*-trimethylammonium)hexyl)fluorene]) (**28**, see Scheme 17) would influence device performance.[143]

We chose to fabricate LEDs using poly[2-methoxy-5-(2′-ethylhexyloxy)-1,4-phenylenevinylene] (MEH-PPV) as the emissive layer because it is an excellent singlet emitter and of its extensive previous characterization and ease of purification.[144] The MEH-PPV was deposited from toluene on a PEDOT-treated ITO surface. Subsequently, a 10 nm film of **28-X** (here **X** refers to a generic anion) was spun-coated from methanol. Finally, an Al or Ba layer was evaporated to serve as the cathode. Figure 11a shows the current density−luminance−voltage (*J*−*L*−*V*) characteristics of control devices with Ba or Al cathodes. Consistent with previous literature work,[145] the better match of the Ba work function (2.7 eV) with the MEH-PPV LUMO (2.9 eV) results in an ohmic contact (i.e., without a barrier) for electron injection and LEDs with higher luminance than these with Al cathodes (work function = 4.3 eV). Figure 11b compares the device characteristics with **28-X**/Al cathodes. These data show that, for **28-Br** (i.e., **28** with bromide counterions) and **28-BAr$^F_4$**, the *J*−*L*−*V* curves do not provide an improvement relative to the MEH-PPV/Al device. However, with **28-CF$_3$SO$_3$** or **28-BIm$_4$**, the *J*−*L*−*V* characteristics are

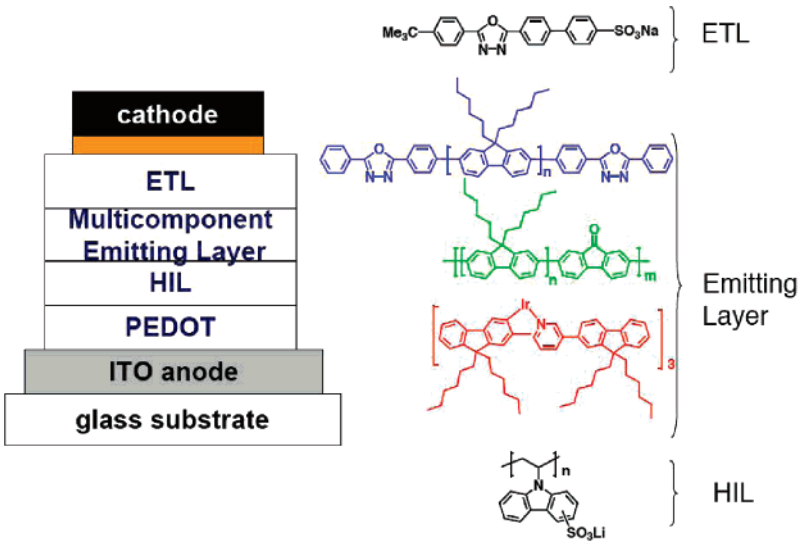

FIGURE 10. Schematic drawing of the white-emitting device structure and molecular structures of the components of selected layers.

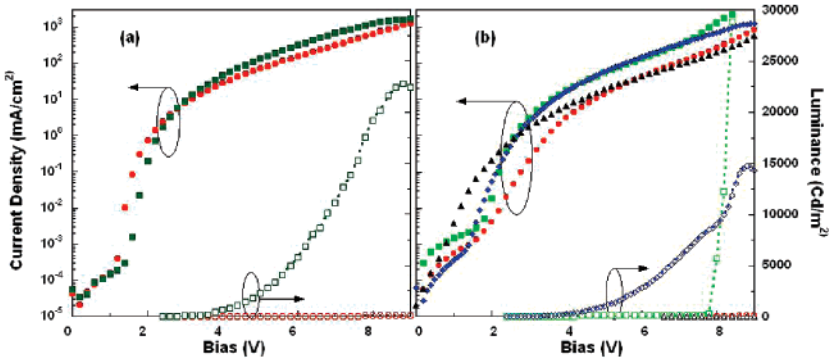

FIGURE 11. *J*−*L*−*V* characteristics of LEDs; (a) ITO/PEDOT/MEH-PPV/Al (red circles) and ITO/PEDOT/MEH-PPV/Ba/Al (green squares); (b) device configuration ITO/PEDOT/MEH-PPV/**28-X**/Al: **28-Br** (red circles), **28-CF_3SO_3** (green squares), **28-BIm_4** (blue diamonds), and **28-BAr^F_4** (black triangles).

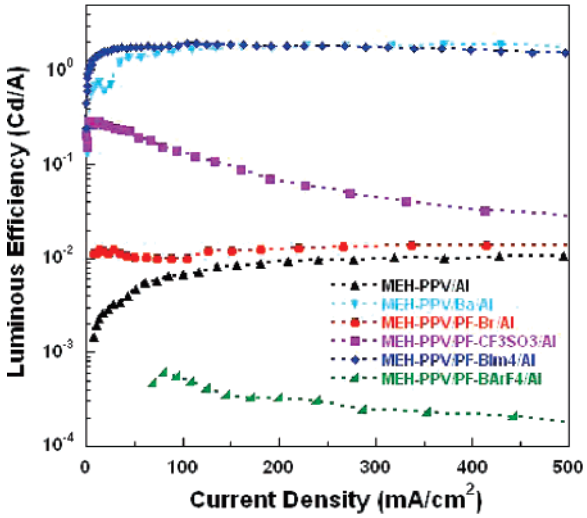

FIGURE 12. Luminous efficiency versus current density characteristics for different cathodes: **28-BAr^F_4**/Al (green), Al (black), **28-Br**/Al (red), **28-CF_3SO_3**/Al (purple), Ba (light blue), and **28-BIm_4**/Al (blue).

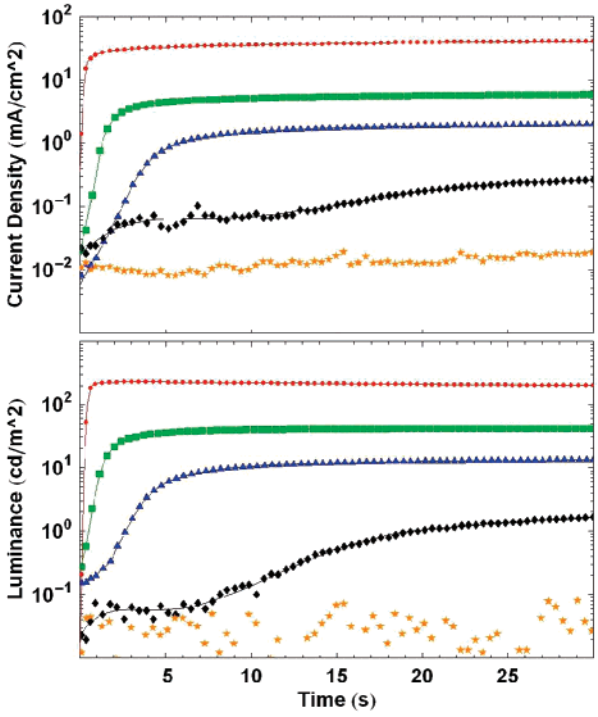

FIGURE 13. Time response of (a) *J* and (b) *L* for an ITO/PEDOT/poly(fluorene)/**22-BIm_4**/Al LED with constant applied bias: 6 V (red circles), 5 V (green squares), 4.5 V (blue triangles), 4 V (black diamonds). Shown in orange stars are the data from a device without the **22-BIm_4** layer at an applied bias of 5 V.

substantially improved, with turn on voltages (the point at which 0.1 cd/m^2 is observed) at the band gap energy (i.e., HOMO−LUMO gap) of MEH-PPV (2.2 eV).

Examination of the light output as a function of injected charges provides for a simple comparison of how the anions influence device characteristics. As shown in Figure 12, the efficiencies up to 500 mA/cm^2 can be ranked in the order (**28-BAr^F_4**/Al) < Al ∼ (**28-Br**/Al) < (**28-CF_3SO_3**/Al) < Ba ∼ (**28-BIm_4**/Al). The efficiencies of devices fabricated with **28-BIm_4**/Al are comparable to those with a Ba cathode. At the other extreme, **28-BAr^F_4**/Al yields devices that are less efficient than those with Al cathodes. Both **28-BIm_4** and **28-BAr^F_4** have identical polymer backbones. Thus, the difference in performance is not due to differences in electrode work function/semiconductor LUMO energy levels.

Figures 11 and 12 demonstrate unambiguously that the performance of conjugated polyelectrolytes as the ETL in PLEDs is strongly influenced by the charge-compensating ions. From a practical perspective, it is possible to find suitable species that allow the use of higher work function, and thus more stable, metals, such as Al, and achieve efficiencies similar to those obtained with Ba. However, these results opened up several basic science questions. In particular, the precise role of the ions continue to be poorly understood. One possibility we considered was that function was limited by ion mobility. Here we expected that the charge-compensating species would migrate within a rigid polymer matrix upon application of an external field. This hypothesis was tested in collaboration with the research group of Professor Thuc-Quyen Nguyen by fabricating PLEDs that contained **22-BIm_4** as the ETL and poly(fluorene) as the emitting layer; the overall device structures were similar to those in Figure 11.[146] Figure 13a shows how *J* develops over time at different applied voltages for a device containing a 10 nm thick **22-BIm_4** layer. A low current is initially observed, which increases up to a limiting value. Faster response times and higher steady state *J* values are attained when the applied voltage is increased. The luminance characteristics for these devices are shown in Figure 13b. Similar behavior to

SCHEME 18. Chemical Structures of Conjugated Polyelectrolytes of the Type 29-X

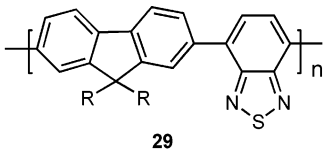

29

R = $(CH_2)_6NMe_3^{\oplus}\ X^{\ominus}$

X = Br, BF_4, CF_3SO_3, PF_6, $B(C_6H_5)_4$ (BPh_4), $B(3,5\text{-}(CF_3)_2C_6H_3)_4$ ($BAr^F{}_4$)

the *J* versus time response is observed: higher brightness and lower response times occur as one increases the applied bias.

The observation of a time response for *J* in the regime of seconds, together with the similar time response for *L*, upon introduction of the **22-BIm$_4$** layer, is consistent with ion motion mediating the device performance and, in particular, the electron injection barrier. Such dependence is difficult to accommodate within a model where the effective work function of the cathode is modified by the presence of a permanent dipole at the cathode interface. In conventional PLEDs, the electroluminescent response is on the nanosecond or microsecond time scales.[147−149] It is useful to note here that we had shown previously how **22-Br** can be used in single-component light-emitting electrochemical cells (LECs).[150] In LECs, the ion motion redistributes the field within the device and compensates the injected charges.[151] The response time in LECs is affected by the mobility of the ions, the distance the ions must traverse, and the magnitude of the electric field,[152] very much like the dependence shown in Figure 13. The action of the polyelectrolyte ETL thus leads to a hybrid device that combines features of PLEDs and LECs and involves mixed ionic and electronic conduction. The time response due to ion motion may provide challenges in nonstatic displays but should not be a significant concern when considering white-emitting PLEDs for solid-state lighting applications.

As demonstrated above, simple ion exchange procedures can be applied to modify the properties of conjugated polyelectrolytes. A given backbone can serve to provide a family of materials. One of our interests was to probe a little deeper on the effect of ions on the basic physical properties of conjugated polyelectrolytes.[153] The bromide ions in poly[(9,9-bis(6′-*N*,*N*,*N*-trimethylammoniumbromide)hexyl)fluorene-*co*-*alt*-4,7-(2,1,3-benzothiadiazole)] (**29** in Scheme 18) were exchanged with BF_4^-, $CF_3SO_3^-$, PF_6^-, BPh_4^-, and $BAr^F{}_4^-$. Absorption, PL, and PL quantum yields were measured in different solvents and in solid films cast from methanol. Examination of the resulting trends, together with the spectral bandshapes in different solvents, suggests that increasing the counteranion size decreases interchain contacts and aggregation and leads to a substantial increase of the emission efficiency in the bulk. Size analysis of polymers containing Br^- and $BAr^F{}_4^-$ in water by dynamic light scattering techniques indicates suppression of aggregation by $BAr^F{}_4^-$.

Nanoscale characterization by C-AFM showed that the presence of the ionic component does not negatively impact charge transport mobility. Indeed, the mobilities are higher for **29-Br** and **29-BAr$^F{}_4$** when compared to those of a neutral conjugated polymer of similar backbone structure, despite possible expectations that the ions may behave as traps for the charge carriers. The higher mobility for **29-Br**, relative to that of **29-BAr$^F{}_4$**, may be accounted for by the tighter interchain contacts that result with the smaller ion. Charge injection barriers are strongly perturbed by the counterion. Specifically, we observed both forward and reverse bias injection *only* with **29-Br**. The ionic component in conjugated polyelectrolytes thus provides a versatile structural handle to fine-tune properties relevant to optoelectronic applications, a fact that has not been widely recognized.

Summary

Control over the atomic connectivity in the constituents of organic materials is provided by the bond-breaking and -forming reactions that organic chemistry has to offer. Reactions that enable new transformations are critical for increasing the types of materials that can be envisioned and ultimately incorporated into new technologies. Controlling the organization of the organic optoelectronic units in the bulk to optimize bulk properties is more difficult at this stage. Furthermore, evaluation of a material from device performance is challenging since a composite picture of multiple components and physical processes is provided. Here the organic chemist needs to reach out to other areas of science.

The work on [2.2]paracyclophanes provides an example of how well-defined organic molecules can be used as study models to unravel complex phenomena in optical and electronic materials. This precise definition within an admittedly simple "aggregate" is useful for gauging theory and characterization techniques. Conjugated polyelectrolytes have less precision but more function. It is worthwhile noting how they can be applied in two typically nonintersecting technologies, biosensors and light-emitting devices.

The work described in this Perspective was accomplished with an excellent group of students, postdoctoral associates, and collaborators. I recognize that group members often need to take a leap of faith in collaborative work. Their synthetic target is often the beginning of the study program. Subsequent characterization and evaluation can take some time, and we are not always successful in providing a well-described picture of how the molecular composition of their materials leads to new knowledge or improved function. I am very grateful for all the effort, patience, energy, confidence, and perseverance from all group members.

Acknowledgment. I am grateful to the National Science Foundation, the Department of Energy, the Office of Naval Research, the Mitsubishi Chemical Center for Advanced Materials, and the Institute for Collaborative Bioctechnologies for financial support of this work.

References

(1) Nicolau, K. C. *J. Org. Chem.* **2005**, *70*, 7007.
(2) Nguyen, T.-Q.; Martini, I. B.; Liu, J.; Schwartz, B. J. *J. Phys. Chem. B* **2000**, *104*, 237.
(3) Shaheen, S. E.; Brabec, C. J.; Sariciftci, N. S.; Padinger, F.; Fromherz, T.; Hummelen, J. C. *Appl. Phys. Lett.* **2001**, *78*, 841.
(4) Coakley, K. M.; McGehee, M. D. *Chem. Mater.* **2004**, *16*, 4533.
(5) Schwartz, B. J. *Annu. Rev. Phys. Chem.* **2003**, *54*, 141.
(6) (a) Burroughes, J. H.; Bradley, D. D. C.; Brown, A. R.; Marks, R. N.; Mackay, K.; Friend, R. H.; Burns, P. L; Holmes, A. B. *Nature* **1990**, *347*, 539. (b) Gustaffson, G.; Cao, Y.; Treacy, G. M.; Klavetter, F.; Colaneri, N.; Heeger, A. J. *Nature* **1992**, *357*, 477.
(7) (a) Tretiak, S.; Zhang, W. M.; Chernyak, V.; Mukamel, S. *Proc. Natl. Acad. Sci. U.S.A.* **1999**, *96*, 13003. (b) Strickler, S. J.; Cormier, R. A.; Connolly, J. S. *Int. J. Quantum Chem.* **1991**, *39*, 345. (c) Scholes, G. D.; Ghiggino, K. P.; Oliver, A. M.; Paddon-Row, M. N. *J. Am. Chem. Soc.* **1993**, *115*, 4345. (d) Clayton, A. H. A.; Scholes, G. D.; Ghiggino, K. P.; Paddon-Row, M. N. *J. Phys. Chem.* **1996**, *100*, 10912.

(8) Gilbert, A.; Baggott, J. *Essentials of Molecular Photochemistry*; CRC Press: Boca Raton, FL, 1991.
(9) Pope, M.; Swenberg, C. E. *Electronic Processes in Organic Crystals*; Clarendon Press: New York, 1982.
(10) (a) Special issue on Light-Harvesting Physics Workshop. *J. Phys. Chem. B* **1997**, *101*. (b) Sundström, V.; van Grondelle, R. In *Anoxygeneic Photosynthetic Bacteria*; Blankenship, R. E., Madiga, M. T., Baner, C. E., Eds.; Kluwer Academic: Dordrecht, The Netherland, 1995; p 349. (c) Hu, X.; Damjanovic, A.; Ritz, T.; Schulten, K. *Proc. Natl. Acad. Sci. U.S.A.* **1998**, *95*, 5935. (d) Linnanto, J.; Helenius, V. M.; Oksanen, J. A. I.; Peltola, T.; Garaud, J.-L.; Korppi-Tommola, J. E. I. *J. Phys. Chem. A* **1998**, *102*, 4337.
(11) (a) Lewis, F. D.; Wu, T.; Zhang, Y.; Letsinger, R. L.; Greenfield, S. R.; Wasielewski, M. R. *Science* **1997**, *277*, 673. (b) Armitage, B. *Chem. Rev.* **1998**, *98*, 1171. (c) Meggers, E.; Michel-Beyerle, M. E.; Giese, B. *J. Am. Chem. Soc.* **1998**, *120*, 12950. (d) Lewis, F. D.; Wu, T.; Liu, X.; Letsinger, R. L.; Greenfield, S. R.; Miller, S. E.; Wasielewski, M. R. *J. Am Chem. Soc.* **2000**, *122*, 2889.
(12) (a) Schuster, G. B. *Acc. Chem. Res.* **2000**, *33*, 253. (b) Beratan, D. N.; Priyadarshy, S.; Risser, S. M. *Chem. Biol.* **1997**, *4*, 3. (c) Turro, N. J.; Barton, J. K. *J. Biol. Inorg. Chem.* **1998**, *3*, 201. (d) Henderson, P. T.; Jones, D.; Hampikian, G.; Kan, Y.; Schuster, G. B. *Proc. Natl. Acad. Sci. U.S.A.* **1999**, *96*, 8353.
(13) Chromophores studied in this manner include: (a) phenanthrenophane: Schweitzer, D.; Hausser, K. H.; Haenel, M. *Chem. Phys.* **1978**, *29*, 181. (b) Anthracenophane: Ishikawa, S.; Nakamura, J.; Iwata, S.; Sumitami, M.; Nagakura, S.; Sakata, Y.; Misumi, S. *Bull. Chem. Soc. Jpn.* **1979**, *52*, 1346. (c) Fluorenophane: Haenel, M. W. *Tetrahedron Lett.* **1976**, *36*, 3121. (d) Colpa, J. P.; Hausser, K. H.; Schweitzer, D. *Chem. Phys.* **1978**, *29*, 187. (e) Pyrenophane and several isomers of naphthalenophane: Haenel, M.; Staab, H. A. *Chem. Ber.* **1973**, *106*, 2190; Otsubo, T.; Mizogami, S.; Osaka, N.; Sakata, Y.; Misumi, S. *Bull. Chem. Soc. Jpn.* **1977**, *50*, 1858. (f) Stilbenophanes: Anger, I.; Sandros, K.; Sundahl, M.; Wennerström, O. *J. Phys. Chem.* **1993**, *97*, 1920; Tsuge, A.; Nishimoto, T.; Uchida, T.; Yasutake, M.; Moriguchi, T.; Sakata, K. *J. Org. Chem.* **1999**, *64*, 7246. (g) Phthalocyanines: de la Escosura, A.; Claessens, C. G.; Ledoux-Rak, I.; Zyss, J.; Martinez-Dias, M. V.; Torres, T. *J. Porphyrins Phthalocyanines* **2005**, *9*, 788.
(14) For studies of cycloaddition reactions, see: (a) Grieving, H.; Hopf, H.; Jones, P. G.; Bubenitscheck, P.; Desvergne, J. P.; Bouass-Laurent, J. *J. Chem. Soc., Chem. Commun*. **1994**, *9*, 1075. (b) Okada, Y.; Ishii, F.; Akiyama, I.; Nishimura, J. *Chem. Lett.* **1992**, *8*, 1579. (c) Grieving, H.; Hopf, H.; Jones, P. G.; Bubenitscheck, P.; Desvergne, J. P.; Bouass-Laurent, J. *Liebigs. Ann.* **1995**, *11*, 1949.
(15) Gleiter, R.; Hopf, H. *Modern Cyclophane Chemistry*; Wiley-VCH: Weinheim, Germany, 2004.
(16) Oldham, W. J.; Miao, Y.-J.; Lachicotte, R. J.; Bazan, G. C. *J. Am. Chem. Soc.* **1998**, *120*, 419.
(17) Bazan, G. C.; Oldham, W. J.; Lachicotte, R. J.; Tretiak, S.; Chernyak, V.; Mukamel, S. *J. Am. Chem. Soc.* **1998**, *120*, 9188.
(18) Birks, J. B. *Photophysics of Aromatic Molecules*; Wiley-Interscience: London, 1970.
(19) The forbidden state has been described in: Canuto, S.; Zerner, M. C. *J. Am. Chem. Soc.* **1990**, *112*, 2114.
(20) Voegtle, F. *Cyclophane Chemistry*; J. Wiley & Sons: New York, 1993.
(21) (a) Reich, H. J.; Cram, D. J. *J. Am. Chem. Soc.* **1969**, *91*, 3534. (b) Izuoka, A.; Murata, S.; Sugawara, T.; Iwamura, H. *J. Am. Chem. Soc.* **1987**, *109*, 2631.
(22) Heck, R. F. *Org. React.* **1982**, *27*, 345.
(23) Beletskaya, I. P.; Cheprakov, A. V. *Chem. Rev.* **2000**, *100*, 3009.
(24) Bartholomew, G. P.; Bazan, G. C. *Acc. Chem. Res.* **2001**, *34*, 30.
(25) Wang, S.; Bazan, G. C.; Tretiak, S.; Mukamel, S. *J. Am. Chem. Soc.* **2000**, *122*, 1289.
(26) For details of this computational technique, see: (a) Takahashi, A.; Mukamel, S. *J. Chem. Phys.* **1994**, *100*, 2366. (b) Mukamel, S.; Takahashi, A.; Wang, H. X.; Chen, G. *Science* **1994**, *266*, 250. (c) Chernyak, V.; Mukamel, S. *J. Chem. Phys.* **1996**, *104*, 444. (d) Mukamel, S.; Tretiak, S.; Wagersreiter, T.; Chernyak, V. *Science* **1997**, *277*, 781. (e) Tretiak, S.; Chernyak, V.; Mukamel, S. *Chem. Phys. Lett.* **1996**, *259*, 55. (f) Tretiak, S.; Chernyak, V.; Mukamel, S. *J. Chem. Phys.* **1996**, *105*, 8914.
(27) (a) Joffre, M.; Yaron, D.; Silbey, R. J. *J. Chem. Phys.* **1992**, *97*, 5607. (b) Zyss, J. *J. Chem. Phys.* **1993**, *98*, 6583.
(28) Bartholomew, G. P.; Ledoux, I.; Mukamel, S.; Bazan, G. C.; Zyss, J. *J. Am. Chem. Soc.* **2002**, *124*, 13480.
(29) Bartholomew, G. P.; Bazan, G. C. *J. Am. Chem. Soc.* **2002**, *124*, 5183.
(30) Zyss, J.; Ledoux, I.; Volkov, S.; Chernyak, V.; Mukamel, S.; Bartholomew, G. P.; Bazan, G. C. *J. Am. Chem. Soc.* **2000**, *122*, 11956.
(31) (a) Terhune, R. W.; Maker, P. D.; Savage, C. M. *Phys. Rev. Lett.* **1965**, *14*, 681. (b) Maker, P. D. *Phys. Rev. Lett.* **1970**, *1*, 923.
(32) Oudar, J.-L. *Chem. Phys.* **1977**, *67*, 446.
(33) Strickler, J. H.; Webb, W. W. *Opt. Commun.* **1991**, *16*, 1780.
(34) Cumpston, B. H.; Ananthavel, S. P.; Barlow, S.; Dyer, D. L.; Ehrlich, J. E.; Erskine, L. L.; Heikal, A. A.; Kuebler, S. M.; Lee, I.-Y. S.; McCord-Maughon, D.; Qin, J.; Röckel, H.; Rumi, M.; Wu, X.-L.; Marder, S. R.; Perry, J. W. *Nature* **1999**, *398*, 51.
(35) Stiel, H.; Teuchner, K.; Paul, A.; Freyer, W.; Leupold, D. *J. Photochem. Photobiol. A* **1994**, *80*, *289*.
(36) Bhawalkar, J. D.; Kumar, N. D.; Zhao, C.-F.; Prasad, P. N. *J. Clin. Laser Surg.* **1997**, *15*, *201*.
(37) (a) Bhawalkar, J. D.; He, G. S.; Prasad, P. N. *Rep. Prog. Phys.* **1996**, *59*, 1041. (b) He, G. S.; Xu, G. C.; Prasad, P. N.; Reinhardt, B. A.; Bhatt, J. C.; Dillard, A. G. *Opt. Lett.* **1995**, *20*, 435.
(38) (a) Ehrlich, J. E.; Wu, X.-L.; Lee, L.-Y.; Hu, Z.-Y.; Röckel, H.; Marder, S. R.; Perry, J. W. *Opt. Lett.* **1997**, *22*, 1843. (b) Ehrlich, J. E.; Wu, X.-L.; Lee, I.-Y. S.; Hu, Z.-Y.; Röckel, H.; Marder, S. R.; Perry, J. W. In *Materials Researcg Society Symposium Proceedings: Materials for Optical Limiting II*; Sutherland, R., Patcher, R., Hood, P., Hagan, D., Lewis, K., Perry, J. W., Eds.; MRS: Pittsburgh, PA, 1997; Vol. 479, pp 9−15.
(39) Fleitz, P. A.; Brant, M. C.; Sutherland, R. L.; Strohkendl, F. P.; Larson, J. R.; Dalton, L. R. *Proc. SPIE Int. Soc. Opt. Eng.* **1998**, *91*, 3472.
(40) Maruo, S.; Nakamura, O.; Kawata, S. *Opt. Lett.* **1997**, *22*, 132.
(41) (a) Zhou, W. H.; Kuebler, S. M.; Braun, K. L.; Yu, T. Y.; Cammack, J. K.; Ober, C. K.; Perry, J. W.; Marder, S. R. *Science* **2002**, *296*, 1106. (b) Stellacci, F.; Bauer, C. A.; Meyer-Friedrichsen, T.; Wenseleers, W.; Alain, V.; Kuebler, S. M.; Pond, S. J. K.; Zhang, Y. D.; Marder, S. R.; Perry, J. W. *Adv. Mater.* **2002**, *14*, 194.
(42) (a) Sun, H. B.; Tanaka, T.; Takada, K.; Kawata, S. *Appl. Phys. Lett.* **2001**, *79*, 1411. (b) Kawata, S.; Sun, H. B.; Tanaka, T.; Takada, K. *Nature* **2001**, *412*, 697.
(43) (a) Miwa, M.; Juodkazis, S.; Kawakami, T.; Matsuo, S.; Misawa, H. *Appl. Phys. A* **2001**, *73*, *561*. (b) Strickler, J. H.; Webb, W. W. *Proc. SPIE Int. Soc. Opt. Eng.* **1990**, *1398*, 107. (c) Wu, E. S.; Strickler, J. H.; Harrell, W. R.; Webb, W. W. *Proc. SPIE Int. Soc. Opt. Eng.* **1992**, *1674*, 776.
(44) Albota, M.; Beljonne, D.; Brédas, J.-L.; Ehrlich, J. E.; Fu, J.-Y.; Heikal, A. A.; Hess, S. E.; Kogej, T.; Levin, M. D.; Marder, S. R.; McCord-Maughon, D.; Perry, J. W.; Röckel, H.; Rumi, M.; Subramaniam, G.; Webb, W. W.; Wu, X.-L.; Xu, C. *Science* **1998**, *281*, 1653.
(45) Bartholomew, G. P.; Rumi, M.; Pond, S. J. K.; Perry, J. W.; Tretiak, S.; Bazan, G. C. *J. Am. Chem. Soc.* **2004**, *126*, 11529.
(46) Silinsh, E. A.; Capek, V. *Organic Molecular Crystals*; AIP Press: New York, 1994.
(47) Denk, W.; Strickler, J. H.; Webb, W. W. *Science* **1990**, *248*, 73.
(48) So, P. T. C.; Dong, C. Y.; Masters, B. R.; Berland, K. M. *Annu. Rev. Biomed. Eng.* **2000**, *2*, *399*.
(49) Oheim, M.; Michael, D. J.; Geisbauer, M.; Madsen, D.; Chow, R. H. *Adv. Drug Delivery Rev.* **2006**, *58*, 788.
(50) Zipfel, W. R.; Williams, R. M.; Webb, W. W. *Nat. Biotechnol.* **2003**, *21*, 1369.
(51) (a) Xu, C.; Williams, R. M.; Zipfel, W.; Webb, W. W. *Bioimaging* **1996**, *4*, 198. (b) Xu, C.; Webb, W. W. *J. Opt. Soc. Am. B* **1996**, *13*, 481. (c) Margineanu, A.; Hofkens, J.; Cotlet, M.; Habuchi, S.; Stefan, A.; Qu, J.; Kohl, C.; Müllen, K.; Vercammen, J.; Engelborghs, Y.; Gensch, T.; Schryver, F. C. D. *J. Phys. Chem. B* **2004**, *108*, 12242.
(52) Xu, C.; Zipfel, W.; Shear, J. B.; Williams, R. M.; Webb, W. W. *Proc. Natl. Acad. Sci. U.S.A.* **1996**, *93*, 10763.
(53) Zojer, E.; Beljonne, D.; Kogej, T.; Vogel, H.; Marder, S. R.; Perry, J. W.; Brédas, J.-L. *J. Chem. Phys.* **2002**, *116*, 3646.
(54) (a) Strehmel, B.; Sarker, A. M.; Malpert, J. H.; Strehmel, V.; Seifert, H.; Neckers, D. C. *J. Am. Chem. Soc.* **1999**, *121*, 1226. (b) Jager, W. F.; Volkers, A. A.; Neckers, D. C. *Macromolecules* **1995**, *28*, 8153.
(55) Schuddeboom, W.; Jonker, S. A.; Warman, J. M.; Leinhos, U.; Kühnle, W.; Zachariasse, K. A. *J. Phys. Chem.* **1992**, *96*, 10809.
(56) The donor strength order is consistent with the oxidation potential measured by cyclic voltammetry.
(57) Cho, B. R.; Son, K. H.; Lee, S. H.; Song, Y.-S.; Lee, Y.-K.; Jeon, S.-J.; Choi, J. H.; Lee, H.; Cho, M. *J. Am. Chem. Soc.* **2001**, *123*, 10039.
(58) Turro, N. J.; Barton, J. K.; Tomalia, D. A. *Acc. Chem. Res*. **1991**, *24*, 332.
(59) (a) *Solution Chemistry of Surfactants*; Mittal, K. L., Ed.; Plenum: New York, 1979. (b) *Micellization, Solubilization, and Microemulsions*; Mittal, K. L., Ed.; Plenum: New York, 1977.
(60) (a) Maciejewski, A.; Kubicki, J.; Dobek, K. *J. Phys. Chem. B* **2003**, *107*, 13986. (b) Fendler, J. H. *Membrane Mimetic Chemistry*; Wiley-Interscience; New York, 1982.
(61) (a) Chakraborty, H.; Sarkar, M. *Langmuir* **2004**, *20*, 3551. (b) Soboleva, I. V.; van Stam, J.; Dutt, G. B.; Kuzmin, M. G.; De Schryver, F. C. *Langmuir* **1999**, *15*, 6201. (c) Arkin, M. R.; Stemp, E. D. A.; Turro, C.; Turro, N. J.; Barton, J. K. *J. Am. Chem. Soc.* **1996**, *118*, 2267.
(62) (a) Maciejewski, A.; Kubicki, J.; Dobek, K. *J. Phys. Chem. B* **2005**, *109*, 9422. (b) Nowick, J. S.; Chen, J. S. *J. Am. Chem. Soc.* **1992**, *114*, 1107.
(63) Hong, J. W.; Woo, H. Y.; Liu, B.; Bazan, G. C. *J. Am. Chem. Soc.* **2005**, *127*, 7435.
(64) (a) Xu, C.; Williams, R. M.; Zipfel, W.; Webb, W. W. *Bioimaging* **1996**, *4*, 198. (b) Margineanu, A.; Hofkens, J.; Cotlet, M.; Habuchi, S.; Stefan, A.; Qu, J.; Kohl, C.; Müllen, K.; Vercammen, J.; Engelborghs, Y.; Gensch, T.; Schryver, F. C. D. *J. Phys Chem. B* **2004**, *108*, 12242.
(65) Wang, S.; Gaylord, B. S.; Bazan, G. C. *Adv. Mater.* **2004**, *16*, 2127.
(66) (a) Kosower, E. M. *Acc. Chem. Res.* **1982**, *15*, 259. (b) Balter, A.; Nowak, W.; Pawelkiewicz, W.; Kowalczyk, A. *Chem. Phys. Lett.* **1988**, *143*, 565.

(67) Renak, M. L.; Bartholomew, G. P.; Wang, S.; Ricatto, P. J.; Lachicotte, R. J.; Bazan, G. C. *J. Am. Chem. Soc.* **1999**, *121*, 7787.

(68) The fluorescence spectrum of **17N** in dodecane is identical to that measured in hexanes. Since the polarizability of dodecane is significantly larger ($\alpha = 22.8$ Å^3) than that of hexanes ($\alpha = 11.8$ Å^3), we propose that the dipole of the solvent plays the major role in the solvatochromic shifts. See: (a) Bosque, R.; Sales, J. *J. Chem. Inf. Comput. Sci.* **2002**, *42*, 1154. (b) Böttcher, C. J. F. *Theory of Electric Polarization*; Elsevier Scientific Publishing Company: Amsterdam, 1973.

(69) (a) Castanheira, E. M. S.; Martinho, J. M. G. *Chem. Phys. Lett.* **1991**, *185*, 319. (b) Castanheira, E. M. S.; Martinho, J. M. G. *J. Photochem. Phototobiol. A: Chem.* **1994**, *80*, 151.

(70) Suppan, P.; Ghoneim, N. *Solvatochromism*; The Royal Society of Chemistry: Cambridge, U.K., 1997.

(71) Barltrop, J. A.; Coyle, J. D. *Principles of Photochemistry*; John Wiley and Sons: Chichester, England, 1978.

(72) Nitzan, A.; Ratner, M. A. *Science* **2003**, *300*, 1384.

(73) Seferos, D. S.; Trammell, S. A.; Bazan, G. C.; Kushmerick, J. G. *Proc. Natl. Acad. Sci. U.S.A.* **2005**, *102*, 8821.

(74) (a) Joachim, C.; Gimzewski, J. K.; Aviram, A. *Nature* **2000**, *408*, 541. (b) Kwok, K. S.; Ellenbogen, J. C. *Mater. Today* **2002**, *5*, 28.

(75) Cui, X. D.; Primak, A.; Zarate, X.; Tomfohr, J.; Sankey, O. F.; Moore, A. L.; Moore, T. A.; Gust, D.; Harris, G.; Lindsay, S. M. *Science* **2001**, *294*, 571.

(76) Kushmerick, J. G.; Naciri, J.; Yang, J. C.; Shashidhar, R. *Nano Lett.* **2003**, *3*, 897.

(77) Xu, B.; Tao, N. J. *Science* **2003**, *301*, 1221.

(78) Yaliraki, S. N.; Ratner, M. A. *J. Chem. Phys.* **1998**, *109*, 5036.

(79) Rochefort, A.; Martel, R.; Avouris, P. *Nano Lett.* **2002**, *2*, 877.

(80) Gierschner, J.; Ehni, M.; Egelhaaf, H. J.; Medina, B. M.; Beljonne, D.; Benmansour, H.; Bazan, G. C. *J. Chem. Phys.* **2005**, *123*, 144914.

(81) Yang, G.; Qian, Y.; Engtrakul, C.; Sita, L. R.; Liu, G.-Y. *J. Phys. Chem. B* **2000**, *104*, 9059.

(82) Seferos, D. S.; Banach, D. A.; Alcantar, N. A.; Israelachvilli, J. N.; Bazan, G. C. *J. Org. Chem.* **2004**, *69*, 1110.

(83) Seferos, D. S.; Lay, R. Y.; Plaxco, K. W.; Bazan, G. C. *Adv. Funct. Mater.* **2006**, *16*, 2387.

(84) Porter, M. D.; Bright, T. B.; Allara, D. L.; Chidsey, C. E. D. *J. Am. Chem. Soc.* **1987**, *109*, 3559.

(85) Bondi, A. *J. Phys. Chem.* **1964**, *68*, 441.

(86) Kushmerick, J. G.; Holt, D. B.; Yang, J. C.; Naciri, J.; Moore, M. H.; Shashidhar, R. *Phys. Rev. Lett.* **2002**, *89*, 086802.

(87) Kushmerick, J. G.; Lazorcik, J.; Patterson, C. H.; Shashidhar, R.; Seferos, D. S.; Bazan, G. C. *Nano Lett.* **2004**, *4*, 639.

(88) Szuchmacher Blum, A.; Kushmerick, J. G.; Pollack, S. K.; Yang, J. C.; Moore, M. H.; Naciri, J.; Shashidhar, R.; Ratna, B. *J. Phys. Chem. B* **2004**, *108*, 18124.

(89) Kushmerick, J. G.; Whitaker, C. M.; Pollack, S. K.; Schull, T. L.; Shashidhar, R. *Nanotechnology* **2004**, *15*, S489.

(90) Kushmerick, J. G.; Holt, D. B.; Pollack, S. K.; Ratner, M. A.; Yang, J. C.; Schull, T. L.; Naciri, J.; Moore, M. H.; Shashidhar, R. *J. Am. Chem. Soc.* **2002**, *124*, 10654.

(91) (a) Xue, Y.; Datta, S.; Ratner, M. A. *J. Chem. Phys.* **2001**, *115*, 4292. (b) Derosa, P. A.; Seminario, J. M. *J. Phys. Chem. B* **2001**, *105*, 471. (c) Taylor, J.; Brandbyge, M.; Stokbro, K. *Phys. Rev. Lett.* **2002**, *89*, 138301. (d) Heurich, J.; Cuevas, J. C.; Wenzel, W.; Schon, G. *Phys. Rev. Lett.* **2002**, *88*, 256803.

(92) Lide, D. R. Ed. *CRC Handbook of Chemistry and Physics*; CRC Press: Boca Raton, FL, 1998.

(93) Mantooth, B. A.; Weiss, P. S. *Proc IEEE* **2003**, *91*, 1785.

(94) Love, J. C.; Estroff, L. A.; Kriebel, J. K.; Nuzzo, R. G.; Whitesides, G. M. *Chem. Rev.* **2005**, *105*, 1103.

(95) Wold, D. J.; Frisbie, C. D. *J. Am. Chem. Soc.* **2001**, *123*, 5549.

(96) Holmlin, R. E.; Hagg, R.; Chabinyc, M. L.; Imagilov, R. F.; Cohen, A. E.; Terfort, A.; Rampi, M. N.; Whitesides, G. M. *J. Am. Chem. Soc.* **2001**, *123*, 5075.

(97) Chen, J.; Reed, M. A.; Rawlett, A. M; Tour, J. M. *Science* **1999**, *286*, 1550.

(98) Cai, L. T.; Skulason, H.; Kushmerick, J. G.; Pollack, S. K.; Naciri, J.; Shashidhar, R.; Allara, D. L.; Mallouk, T. E.; Mayer, T. S. *J. Phys. Chem. B* **2004**, *108*, 2827.

(99) (a) Amlnai, I.; Rawlett, A. M.; Nagahara, L. A.; Tsui, R. *Appl. Phys. Lett.* **2002**, *80*, 2761. (b) Long, D. P.; Patterson, C. H.; Moore, M. H.; Seferos, D. S.; Bazan, G. C.; Kushmerick, J. G. *Appl. Phys. Lett.* **2005**, *86*, 153105.

(100) (a) Reed, M. A.; Zhou, C.; Muller, C. J.; Burgin, T. P.; Tour, J. M. *Science* **1997**, *278*, 252. (b) Mayor, M.; Weber, H. B.; von Hanisch, C.; Reichert, J.; Beckman, D. *Angew. Chem., Int. Ed.* **2002**, *41*, 1183.

(101) (a) Bumm, L. A.; Arnold, J. J.; Cygan, M. T.; Dunbar, T. D.; Burgin, T. P.; Jones, L., II; Allara, D. L.; Tour, J. M.; Weiss, P. S. *Science* **1996**, *271*, 1705. (b) Blum, A. S.; Kushmerick, J. G.; Pollack, S. K.; Yang, J. C.; Moore, M.; Naciri, J.; Shashidhar, R.; Ratna, B. R. *J. Phys. Chem. B.* **2004**, *108*, 18124.

(102) Cui, X. D.; Primak, A.; Zarate, X.; Torfohr, J.; Sankey, O. F.; Moore, A. L.; Moore, T. A.; Gust, D.; Harris, G.; Lindsey, S. M. *Science* **2001**, *294*, 571.

(103) Cygan, M. T.; Dunbar, T. D.; Arnold, J. J.; Bumm, L. A.; Shedlock, N. F.; Burgin, T. P.; Jones, II. L.; Allara, D. L.; Tour, J. M.; Weiss, P. S. *J. Am. Chem. Soc.* **1998**, *120*, 2721.

(104) (a) Bumm, L. A.; Arnold, J. J.; Dunbar, T. D.; Allara, D. L.; Weiss, P. S. *J. Phys. Chem. B* **1999**, *103*, 8122. (b) Moth-Poulsen, K.; Patrone, L.; Stuhr-Hansen, N.; Christensen, J. B.; Bourgoin, J. P.; Bjornholm, T. *Nano Lett.* **2005**, *5*, 783. (c) Blum, A. S.; Ren, T.; Parrish, D. A.; Trammell, S. A.; Moore, M. H.; Kushmerick, J. G.; Xu, G.-L.; Deschamps, J. R.; Pollack, S. K.; Shashidhar, R. *J. Am. Chem. Soc.* **2005**, *127*, 10010. (d) Monnell, J. D.; Stapleton, J. J.; Dirk, S. M.; Reinerth, W. A.; Tour, J. M.; Allara, D. L.; Weiss, P. S. *J. Phys. Chem. B* **2005**, *109*, 20343.

(105) Pinto, M. R.; Schanze, K. S. *Synthesis* **2002**, *9*, 1293.

(106) Gaylord, B. S.; Wang, S. J.; Heeger, A. J.; Bazan, G. C. *J. Am. Chem. Soc.* **2001**, *123*, 6417.

(107) Stork, M.; Gaylord, B. S.; Heeger, A. J.; Bazan, G. C. *Adv. Mater.* **2002**, *14*, 361.

(108) (a) McUuade, D. T.; Pullen, A. E.; Swager, T. M. *Chem. Rev.* **2000**, *100*, 2537. (b) Liu, B.; Bazan, G. C. *Chem. Mater.* **2004**, *16*, 4467. (c) Zheng, J.; Swager, T. M. *Adv. Polym. Sci.* **2005**, *177*, *151*. (d) Faïd, K.; Leclerc, M. *Chem. Commun.* **1996**, 2761 (e) Doré, K.; Dubus, S.; Ho, H.-A.; Lévesque, I.; Brunette, M.; Corbeil, G.; Boissinot, M.; Boivin, G.; Bergeron, M. G.; Boudreau, D.; Leclerc, M. *J. Am. Chem. Soc.* **2004**, *126*, 4240. (f) Nilsson, K. P. R.; Inganäs, O. *Macromolecules* **2004**, *37*, 9109. (g) Nilsson, K. P. R.; Rydberg, J.; Baltzer, L.; Inganäs, O. *Proc. Natl. Acad. Sci. U.S.A.* **2003**, *100*, 10170.

(109) (a) Kim, I. B.; Dunkhorst, A.; Gilbert, J.; Bunz, U. H. F. *Macromolecules* **2005**, *38*, 4560. (b) Le Floch, F.; Ho, H. A.; Harding-Lepage, P.; Bedard, M.; Neagu-Plesu, R.; Leclerc, M. *Adv. Mater.* **2005**, *17*, 1251. (c) Ho, H. A.; Bers-Aberem, M.; Leclerc, M. *Chem.—Eur. J.* **2005**, *11*, 1718. (d) Nilsson, K. P. R.; Inganäs, O. *Nat. Mater.* **2003**, *2*, 419. (e) Herland, A.; Nilsson, K. P. R.; Olsson, J. D. M.; Hammarstrom, P.; Konradsson, P.; Inganäs, O. *J. Am. Chem. Soc.* **2005**, *127*, 2317.

(110) (a) Xu, Q.; Wang, S.; Korystov, D.; Mikhailovsky, A.; Bazan, G. C.; Moses, D.; Heeger, A. J. *Proc. Natl. Acad. Sci. U.S.A.* **2005**, *102*, 530. (b) Tang, Y.; Feng, F.; He, F.; Wang, S.; Li, Y.; Zhu, D. *J. Am. Chem. Soc.* **2006**, *128*, 14972.

(111) Cooper, J.; Cass, T. *Biosensors: A Practical Approach*; Oxford University Press: London, 2004.

(112) Thomas, S. W.; Joly, G. D.; Swager, T. M. *Chem. Rev.* **2007**, *107*, 1339.

(113) Dwight, S. J.; Gaylord, B. S.; Hong, J. W.; Bazan, G. C. *J. Am. Chem. Soc.* **2004**, *126*, 16850.

(114) Gaylord, B. S.; Heeger, A. J.; Bazan, G. C. *Proc. Nat. Acad. Sci. U.S.A.* **2002**, *99*, 10954.

(115) Gaylord, B. S.; Massie, M. R.; Feinstein, S. C.; Bazan, G. C. *Proc. Natl. Acad. Sci. U.S.A.* **2005**, *102*, 34.

(116) Lee, V. M-Y.; Goedert, M.; Trojanowski, J. Q. *Annu. Rev. Neurosci.* **2001**, *24*, 1121.

(117) Wang, S.; Bazan, G. C. *Adv. Mater.* **2003**, *15*, 1425.

(118) Gaylord, B. S.; Heeger, A. J.; Bazan, G. C. *J. Am. Chem. Soc.* **2003**, *125*, 896.

(119) He, F.; Tang, Y. L.; Yu, M. H.; Feng, F.; An, L. L.; Sun, H.; Wang, S.; Li, Y. L.; Zhu, D. B.; Bazan, G. C. *J. Am. Chem. Soc.* **2006**, *128*, 6764.

(120) Baker, E. S.; Hong, J. W.; Gaylord, B. S.; Bazan, G. C.; Bowers, M. T. *J. Am. Chem. Soc.* **2006**, *128*, 8484.

(121) Liu, B.; Baudrey, S.; Jaeger, L.; Bazan, G. C. *J. Am. Chem. Soc.* **2004**, *126*, 4076.

(122) Liu, B.; Bazan, G. C. *Proc. Natl. Acad. Sci. U.S.A.* **2005**, *102*, 589.

(123) Förster, T. *Ann. Phys.* **1948**, *2*, 55.

(124) Cornil, J.; Lemaur, V.; Steel, M. C.; Dupin, H.; Burquel, A.; Beljonne, D.; Bredas, J. L. In *Organic Photovoltaics*; Sun, S. J., Sariciftci, N. S., Eds.; Taylor & Francis: Boca Raton, FL, 2005.

(125) (a) Sariciftci, N. S.; Smilowitz, L.; Heeger, A. J.; Wudl, F. *Science* **1992**, *258*, 1474. (b) Marcus, R. A. *Angew. Chem., Int. Ed. Engl.* **1993**, *32*, 1111. (c) Xu, Q. H.; Moses, D.; Heeger, A. J. *Phys. Rev. B* **2003**, *67*, 245417. (d) Brédas, J. L.; Beljonne, D.; Coropceanu, V.; Cornil, J. *Chem. Rev.* **2004**, *104*, 4971. (e) Thomas, K. R. J.; Thompson, A. L.; Sivakumar, A. V.; Bardeen, A. J.; Thayumanavan, S. *J. Am. Chem. Soc.* **2005**, *127*, 373.

(126) Morteani, A. C.; Sreearunothai, P.; Herz, L. M.; Friend, R. H.; Silva, C. *Phys. Rev. Lett.* **2004**, *92*, 247402−1.

(127) Liu, B.; Bazan, G. C. *J. Am. Chem. Soc.* **2006**, *128*, 1188.

(128) Woo, H. Y.; Vak, D.; Korystov, D.; Mikhailovsky, A.; Bazan, G. C.; Kim, D. Y. *Adv. Funct. Mater.* **2007**, *17*, 290.

(129) Turro, N. J. *Modern Molecular Photochemistry*: University Science Books: Mill Valley, CA, 1997.

(130) (a) Tyagi, S.; Kramer, F. R. *Nat. Biotechnol.* **1996**, *14*, 303. (b) Johansson, M. K.; Fidder, H.; Dick, D.; Cook, R. M. *J. Am. Chem. Soc.* **2002**, *124*, 6950.

(131) Götz, M.; Hess, S.; Beste, G.; Skerra, A.; Michel-Beyerle, M. E. *Biochemistry* **2002**, *41*, 4156.

(132) Ma, W. L.; Iyer, P. K.; Gong, X.; Liu, B.; Moses, D.; Bazan, G. C.; Heeger, A. J. *Adv. Mater.* **2005**, *17*, 274.

(133) Wu, H. B.; Huang, F.; Peng, J. B.; Cao, Y. *Org. Electron.* **2005**, *6*, 118.
(134) Edman, L.; Liu, B.; Vehse, M.; Swensen, J.; Bazan, G. C.; Heeger, A. J. *J. Appl. Phys.* **2005**, *98*, 44502.
(135) Parker, I. D. *J. Appl. Phys*. **1994**, *75*, 1665.
(136) Tang, C. W.; Vanslyke, S. A. *Appl. Phys. Lett.* **1987**, *51*, 913.
(137) Ishii, H.; Sugiyama, K.; Ito, E.; Seki, K. *Adv. Mater*. **1999**, *11*, 605.
(138) Shen, Y. L.; Hosseini, A. R.; Wong, M. H.; Malliaras, G. G. *Chem. Phys. Chem.* **2004**, *5*, 16.
(139) Nuyken, O.; Jungermann, S.; Wiederhirn, V.; Bacher, E.; Meerholz, K. *Monatsh. Chem.* **2006**, *137*, 811.
(140) Malliaras, G. G.; Scott, J. C. *J. Appl. Phys.* **1998**, *83*, 5399.
(141) Campbell, I. H.; Joswick, M. D.; Parker, I. D. *Appl. Phys. Lett.* **1995**, *67*, 3171.
(142) Gong, X.; Wang, S.; Moses, D.; Bazan, G. C.; Heeger, A. J. *Adv. Mater*. **2005**, *17*, 2053.
(143) Yang, R. Q.; Wu, H. B.; Cao, Y.; Bazan, G. C. *J. Am. Chem. Soc*. **2006**, *128*, 14422.
(144) Braun, D.; Heeger, A. J. *Appl. Phys. Lett.* **1991**, *58*, 1982.
(145) Cao, Y.; Yu, G.; Parker, I. D.; Heeger, A. J. *J. Appl. Phys.* **2000**, *88*, 3618.
(146) Hoven, C.; Yang, R.; Garcia, A.; Heeger, A. J.; Nguyen, T.-Q.; Bazan, G. C. Submitted.
(147) Book, K.; Nikitenko, V. R.; Bassler, H.; Elschner, A. *Synth. Met.* **2001**, *122*, 135.
(148) Wang, J.; Sun, R. G.; Yu, G.; Heeger, A. J. *Synth. Met.* **2003**, *137*, 1009.
(149) Pinner, D. J.; Friend, R. H.; Tessler, N. *J. Appl. Phys.* **1999**, *86*, 5116.
(150) (a) Cheng, C. H. W.; Lin, F. D.; Lonergan, M. C. *J. Phys. Chem. B* **2005**, *109*, 10168. (b) Cimrova, V.; Schmidt, W.; Rulkens, R.; Schulze, M.; Meyer, W.; Neher, D. *Adv. Mater*. **1996**, *8*, 585. (c) Gu, Z.; Shen, Q. D.; Zhang, J.; Yang, C. Z.; Bao, Y. J. *J. App. Polym. Sci*. **2006**, *100*, 2930. (d) Neher, D.; Gruner, J.; Cimrova, V.; Schmidt, W.; Rulkens, R.; Lauter, U. *Polym. Adv. Technol.* **1998**, *9*, 461.
(151) (a) Pei, Q. B.; Yu, G.; Zhang, C.; Yang, Y.; Heeger, A. J. *Science* **1995**, *269*, 1086. (b) Smith, D. L. *J. Appl. Phys.* **1997**, *81*, 2869.
(152) (a) Pei, Q. B.; Yang, Y.; Yu, G.; Zhang, C.; Heeger, A. J. *J. Am. Chem. Soc.* **1996**, *118*, 3922. (b) Zhang, Q. S.; Zhou, Q. G.; Cheng, Y. X.; Wang, L. X.; Ma, D. G.; Jing, X. B.; Wang, F. S. *Adv. Funct. Mater*. **2006**, *16*, 1203.
(153) Yang, R. W.; Garcia, A.; Korystov, D.; Mikhailovsky, A.; Bazan, G. C.; Nguyen, T.-Q. *J. Am. Chem. Soc.* **2006**, *128*, 16532.

JO071176N